Event correlation analysis of the Galactic Centre region

Author:
Ramin Marx

Supervisors:
Prof. Dr. Werner Hofmann, MPIK
Dr. Henning Gast, MPIK
Prof. Dr. Isabelle Bloch, UPMC
Prof. Dr. Séverine Dubuisson, UPMC

Max-Planck-Institut für Kernphysik, Heidelberg (MPIK)
Université Pierre et Marie Curie, Paris (UPMC)

May 2012

In order to investigate cosmic particle accelerators, like fast rotating neutron stars or supernova remnants, the very-high-energy (VHE: $E > 100$ GeV) γ-radiation generated during these processes is detected by imaging atmospheric Cherenkov telescopes (IACTs). With the H.E.S.S. telescopes, which are an array of four such IACTs located in Namibia, many data sets have already been collected and particularly the Galactic plane has been observed extensively. In the Galactic Centre region, it has detected two strong point sources (G 0.9+0.1 and Sagittarius A*) and an extended band of diffuse emission, located at the position of the giant molecular cloud in the Galactic Centre.
In this work H.E.S.S. data from the Galactic Centre region is analyzed with an event correlation method in order to find out if there are populations of weak sources that cannot be detected individually by classical methods.
First, the event correlation method is compared to the ring background method and then, it is verified in Monte Carlo simulations. For the generation of the required null hypothesis maps different methods that randomize the data at small scales are explained and analyzed. The findings of the simulations then tell how strongly the data may be randomized without changing the large-scale distributions and how many point sources and how many events per source there would have to be in the data in order to get detected.
According to the correlation analysis, there are no small-scale anisotropies in the event distribution, which means that the VHE γ-radiation from the Galactic Centre region (minus the emission from Sagittarius A* and G 0.9+0.1) is consistent with diffuse emission only.

Contents

1 Introduction

1.1 Motivation for VHE γ-ray astronomy

In order to learn more about cosmic objects, astronomers capture the light they emit, which comes in a wide range of energies. Observing these objects with telescopes sensitive to very high energies (VHE; $E > 100$ GeV) enhances our understanding of the universe.
Within these objects, charged particles are accelerated and then react to form VHE γ-rays. Such a particle can be a relativistic p^+ that hits a nucleus, thereby creating a π^0 which then decays to $2\,\gamma$ or an e^- transfering energy to a γ-photon via Inverse Compton Scattering. As the emitted light is neither deflected by electric nor magnetic fields, it conserves the information about its origin even after it transits the Galactic Magnetic Field.

Among the cosmic particle accelerators are:

SNRs (Supernova Remnants): exploded stars whose shock waves transfer kinetic energy to particles over a long period of time (several 1000 years)

PWNe (Pulsar Wind Nebulae): neutron stars with a very short period of rotation and a strong magnetic field, which produces focused beams of charged relativistic particles that hit their surrounding gas cloud

AGN (Active Galactic Nuclei): an AGN is the center region of a galaxy containing a supermassive ($\approx 10^8$ solar masses) black hole, which accelerates matter on its accretion disc and emits relativistic jets

Investigating the mechanisms that lead to particle acceleration is subject of current research and thus, measuring their γ-ray spectrum supplies crucial information.

1.2 Detecting γ-rays

The flux of γ-rays in the TeV-range is so low, approximately 1 particle per m^2 per year, that satellite based detectors with their small detection areas of around 1 m^2 cannot capture significant signals. Ground-based telescopes on the other hand cannot detect γ-rays directly, because the atmosphere is not transparent

to high-energetic photons. But when such a photon enters the atmosphere and interacts with the nucleus of an atom (this happens typically at a height of 10 km), it transforms into an e^- and an e^+ (pair production), which in turn collide with other nuclei generating more γ-photons (Bremsstrahlung). This process continues and generates an air shower of secondary particles moving faster than the speed of light in air.
During their flight these particles emit Cherenkov radiation within an angle of about 1°, which then overlaps and passes the air with little interaction. This blue light flash arrives at the ground and illuminates a circle of $\sim$ 250 m in diameter for a time span of only some nanoseconds. Although it is very weak ($\sim$ 100 photons per m^2), it can be detected with very sensitive photomultiplier tubes.
The camera images are then approximated as ellipses (Hillas-parametrization) and the energy and direction of the photon can be reconstructed. Unfortunately, relativistic hadrons cause similar air showers and thus, similar Cherenkov light patterns are seen by the camera.
Although cuts on the Hillas-parameters can remove more than 99% of the hadronic events, a high background level still remains.

1.3 The H.E.S.S. experiment

H.E.S.S. is a system of four Imaging Atmospheric Cherenkov Telescopes located in Namibia and stands for **H**igh **E**nergy **S**tereoscopic **S**ystem. Its name also refers to Victor Hess, the discoverer of cosmic radiation.
The telescopes are pointed at a position in the sky and counts the arriving events with a field of view of 5°. Its point spread function is a superposition of two Gaussians that depends on the zenith angle, but is here approximated by one Gaussian with a width of just $\sigma_{\mathrm{psf}} = 0.1°$ for tests.
Cosmic rays with energies ranging from 100 GeV to 100 TeV can be detected. Thanks to the huge detector area of 10^5 m^2 the time required for a $5\,\sigma$ detection of a source with the flux of the Crab Nebula is just 30 seconds and since 2002 H.E.S.S. has detected more than 60 Galactic VHE γ-ray sources [6].

1.4 Data

H.E.S.S. provides a list of γ-ray event candidates, whose arrival direction is then used to create an event map of the observed region. In cases where exceptionally many events are located inside of a small area it is very probable that it is a γ-source and the standard analysis methods can confirm a detection. However, often the sources are weak compared to the background level and thus, no significant detection is achieved.

The data used in this work is shown in figure 3.1 (a). It consists of $\sim 300,000$ events distributed around the Galactic Centre

1.5 Analysis of the Galactic Centre region

Investigating the Galactic Centre in order to resolve its composition and to understand the accelerator mechanisms is a current research topic in astroparticle physics. It has been extensively observed with the H.E.S.S. telescopes both during the Galactic Plane survey [4] and during the investigation of the black hole Sagittarius A* [1] and the supernova remnant G 0.9+0.1 [2], in which VHE γ-ray emission from both these sources was detected.
Figure 1.1 shows a γ count map of the Galactic Centre region with Sagittarius A* and G 0.9+0.1 clearly visible. After substraction of these two strong point sources, an extended band of diffuse γ-ray emission becomes visible (see figure 1.2), which is probably caused by accelerated protons and nuclei [3]. The position of the band coincides with the position of the giant molecular cloud (see the white contours indicating its density) found earlier [10].
However, apart from the diffuse emission, there may also be unresolved point sources, whose signals are too faint to be detected individually [7].
Here, a method is studied that estimates the significance of a detection of small-scale anisotropies in the event maps and applies it to the data taken from the Galactic Centre in order to search for populations of weak point sources.

These are the plots published in [3]:

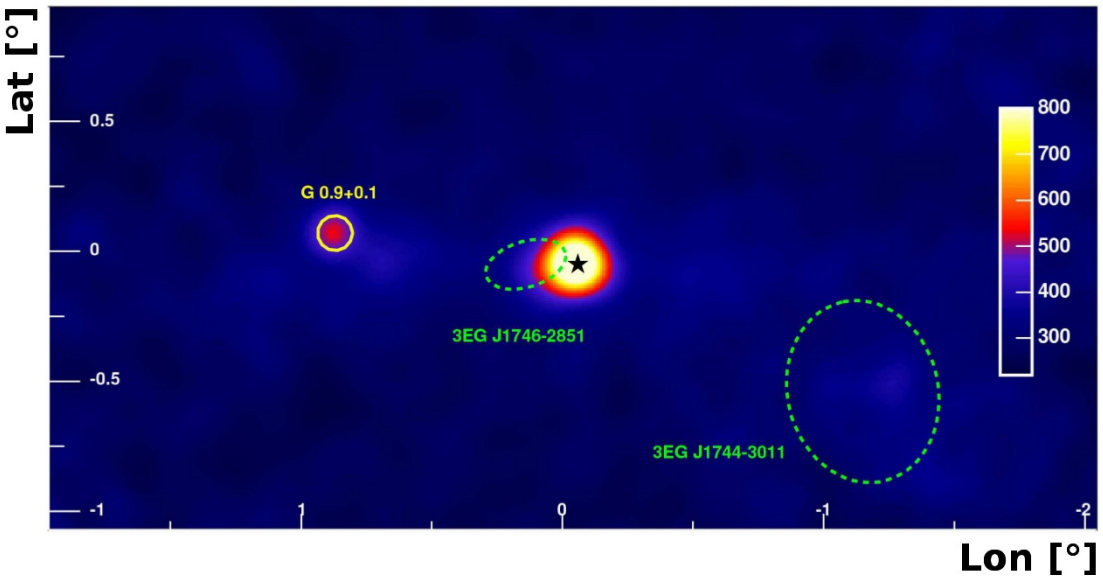

Figure 1.1: Excess map (background removed) of the Galactic Centre region

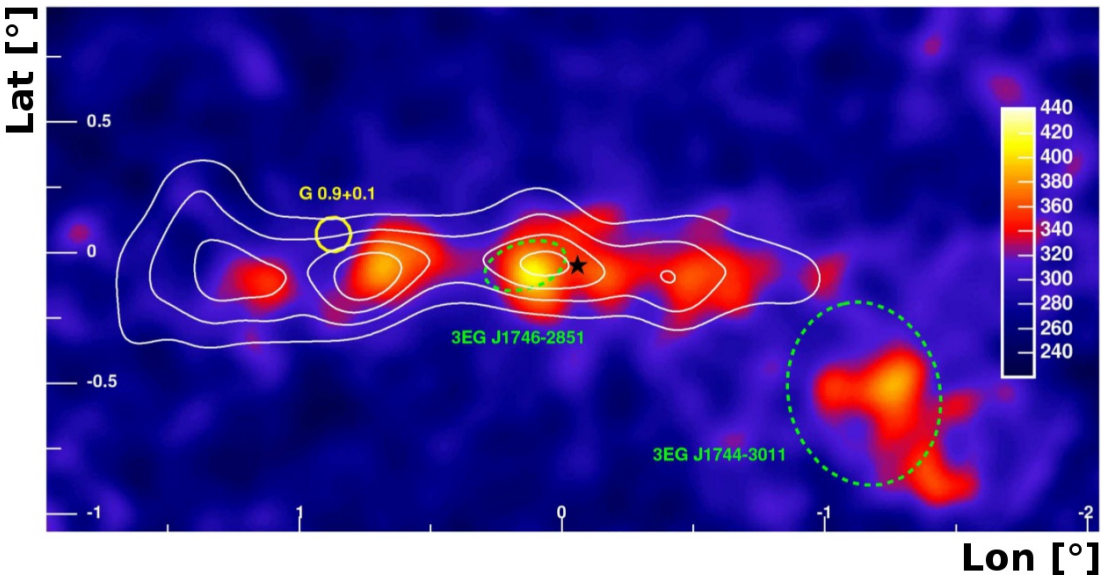

Figure 1.2: Same map after substraction of the two point sources

2 Studying the event correlation method in cases with isotropic background

In this chapter, the *event correlation* method is explained and compared to the *ring background* method by means of toy Monte Carlo simulations. In particular, it is investigated how much the methods benefit from an increased number of sources and source events.
Although the event maps provided by the H.E.S.S. telescopes have complicated background distributions and sources of different strength and morphology, the event maps used in this chapter are extreme simplifications (see 2.3), in order to place emphasis on the characteristics of the analysis methods.

2.1 Ring background method

The *ring background method* is a standard method in γ-ray astronomy for estimating the significance of an excess of events at an arbitrary position x in the field of view by comparing N_{on} (the number of events in an circle around x) with N_{off} (the number of events in a ring around x):

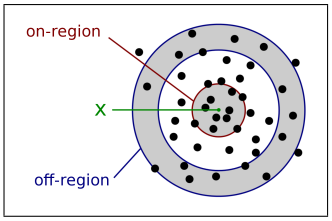

Exemplary sketch of the on- and off-regions used in the ring background method. To include most of the source events, but not too much of the background, the radius of the on-region is chosen to be $r_0 = 1.5\,\sigma_{\text{psf}}$ and the inner radius of the off-region $r_1 = 3\,r_0$. As an area ratio of $\alpha = \frac{1}{7}$ is usually chosen, the outer radius of the off-region can then be calculated to $r_2 = 4\,r_0$. For a detailed description of the ring background method (taking also exposure time etc. into account) see [5].

Combined with the formula proposed by [8],

$$S(N_{\text{on}},\, N_{\text{off}},\, \alpha) = \sqrt{2}\left(N_{\text{on}} \ln\left[\frac{1+\alpha}{\alpha}\,\frac{N_{\text{on}}}{N_{\text{on}}+N_{\text{off}}}\right] + N_{\text{off}} \ln\left[(1+\alpha)\,\frac{N_{\text{off}}}{N_{\text{on}}+N_{\text{off}}}\right]\right)^{\frac{1}{2}} \quad (2.1)$$

the significance of a signal at position x can be calculated and a significance map can be created (see figure 2.1 (b)).

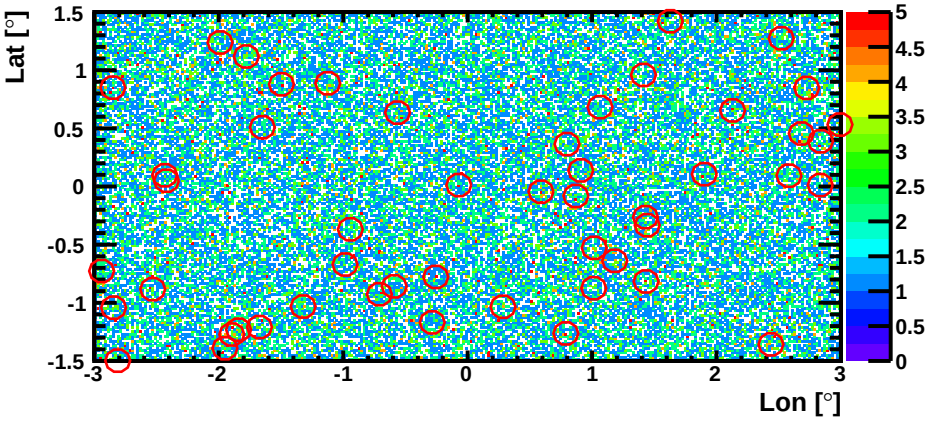

(a) event map

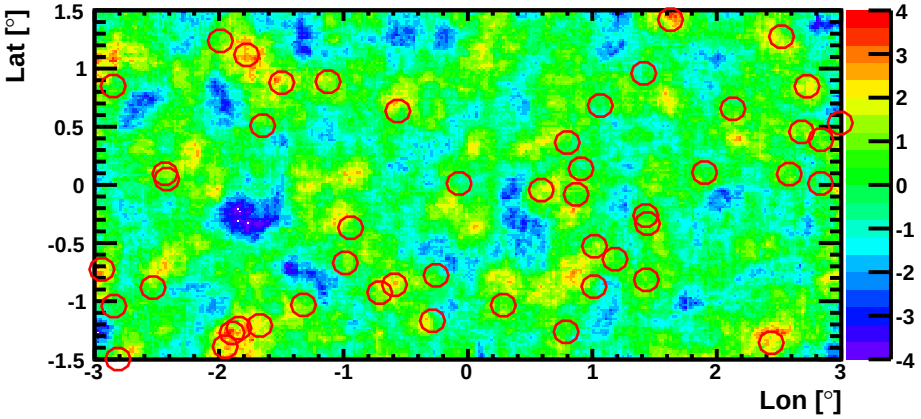

(b) significances of map with sources

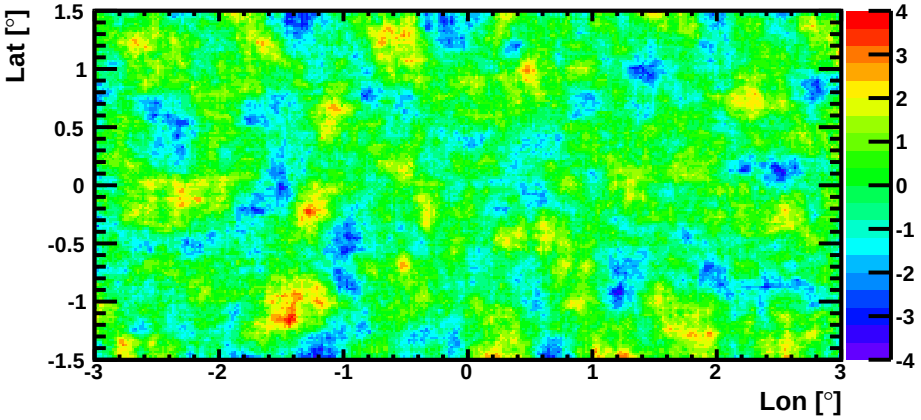

(c) significances of map without sources

Figure 2.1: from top to bottom: binned event map (bin width = 0.02° with 50 sources (marked by red circles) à 20 events on isotropic background (50,000 events altogether), ring background map of the above map showing the Li-Ma-significances (pre-trial) and for comparison the ring background map of a pure isotropic background map with 50,000 events

To correct for fluctuations of the background (see figure 2.1 (c)), a trial factor is usually introduced, which normalizes the Li-Ma-significance by considering the number of tested positions. However, in this study the significances are not scaled by a trial factor, because the detection error measure defined on page 15 already considers this effect.

Since faint sources yield a low significance and every position on the map is examined independently, one would expect that even many weak sources can not be detected with the ring background method. Furthermore, if many sources are placed on the map, the probability of a source being located inside of the ring is increased, leading to a higher background level and lower significances.
Figure 2.2 shows the distribution of the maximum significances obtained with the ring background method if there is a minimum distance of 0.2° between all sources. The detection performance of the ring background method depends on the number of source events, but not on the number of sources, although the probability of a detection might increase slightly with the number of sources, because of the higher probability of a source being located on a region with upwards fluctuating background. In average, a map without any sources contains at least one bin with a significance of more than $4\,\sigma$.

In a more realistic scenario, in which sources may overlap, the ring background method performs better, because the superposition of weak sources resembles one stronger source, leading to higher significances (see figure 2.3). Also, without the constraints of a minimum distance, more sources can fit on a map and maps with up to 100 sources are examined.

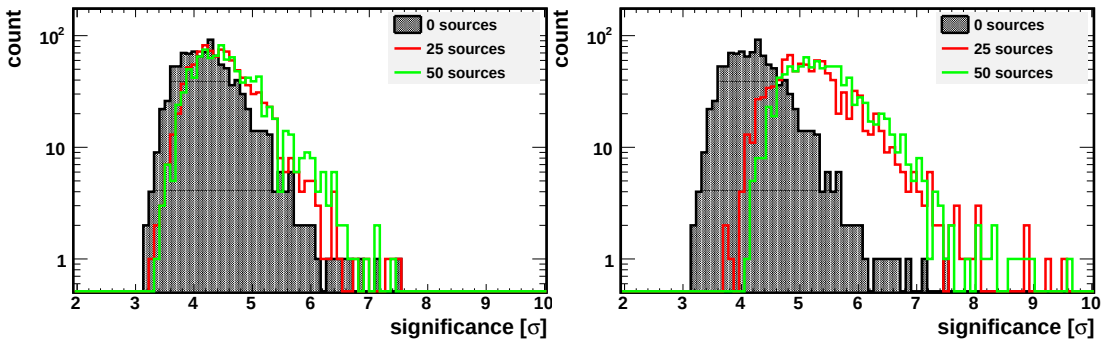

(a) $n_{src.ev} = 20$ (b) $n_{src.ev} = 40$

Figure 2.2: Ring background method: **maximum** significances for maps with and without sources. Minimum distance between two sources is 0.2°. The number of events (source events plus background) is 50,000.

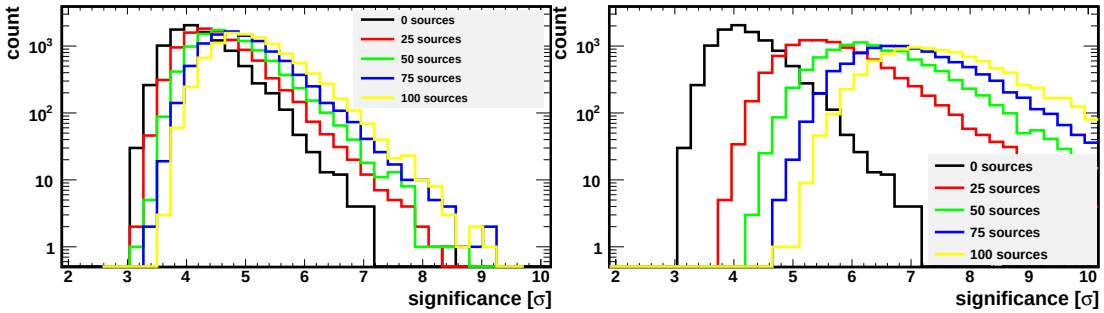

(a) $n_{src.ev} = 20$ (b) $n_{src.ev} = 40$

Figure 2.3: Ring background method: **maximum** significances for maps with and without sources. No minimum distance between two sources is required ⇒ sources may overlap. The number of events (source events plus background) is 50,000.

2.2 Event correlation method

The idea of this method [9] is to consider all events on a map and return a global measure for the deviation from a map with background events only (null hypothesis map). If there are several point sources that are too weak to be detected individually, one could measure the anisotropy of the event distribution at the scale of the point spread function ($\sigma_{\mathrm{psf}} \sim 0.1^\circ$ for H.E.S.S.) and sum up all the contributions of these sources:
Given a map M with n events, every event x_i is regarded as the centre of a possible point source and in a region R^i around it, the distances to all n_i events R^i_j are calculated and stored in a histogram

$$f(M,r) = \frac{1}{N} \sum_{i=1}^{n} \sum_{j=1}^{n_i} \delta(|x_i - R^i_j|, r). \tag{2.2}$$

The regions R^i are circles with a radius of $\sim 2\,\sigma_{\mathrm{psf}}$, which is a good compromise between including most of the events of a possible source and neglecting most of the extrinsic events. The factor $\frac{1}{N}$ normalizes the histogram by dividing by the sum of event pairs in the map with distance smaller than the radius of R.
The correlation function ϕ is then defined as

$$\phi(M,r) = \frac{f(M,r)}{f_0(r)} \text{ , where} \tag{2.3}$$

$$f_0(r) = \frac{1}{n} \sum_{i=1}^{n} f(M^i_0, r) \tag{2.4}$$

is an approximation of the null hypothesis, calculated by averaging the distance distributions of several null hypothesis maps M^i_0. If $\phi(M,r)$ lies significantly above 1, M probably contains anisotropies at angular distances r.
As f shows large fluctuations (see figure 2.4 (a)), it is difficult to choose a fixed r. On the other hand, choosing an arbitrary r in order to maximize the significance demands a trial factor.
A solution is to integrate f and thus stabilizing it:

$$F(M,r) = \sum_{k=1}^{n_{\mathrm{bins}}(r)} f(M, r_k)\,. \tag{2.5}$$

Similarly to ϕ, the correlation function Φ becomes

$$\Phi(M,r) = \frac{F(M,r)}{F_0(r)}\,, \tag{2.6}$$

with F_0 analogously obtained as f_0. Now, if $\Phi(M,r)$ lies significantly above 1, M probably contains anisotropies at angular distances $[0, r[$.

Figure 2.4 (b) shows the integrated correlation function, $\Phi(M, r)$, for maps with and without sources. It is much more stable than ϕ and can distinguish best between random map and map with sources at r $sim0.1°$.
Large r include more source events, but also more background events. That is why r should not be chosen to be much bigger than $\sigma_{\text{psf}} = 0.1°$.

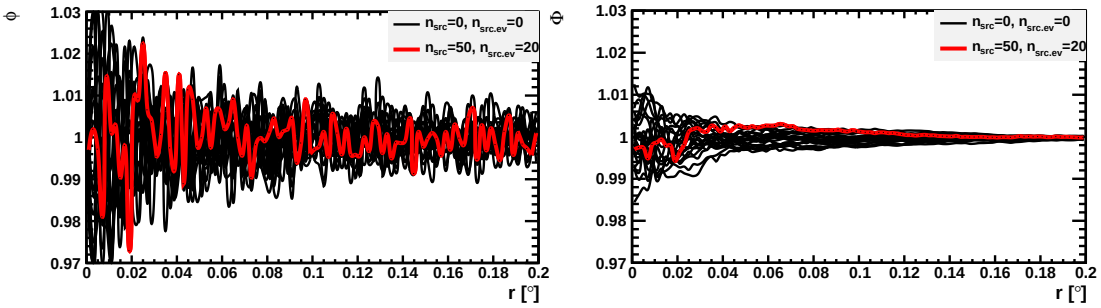

(a) $\phi(M)$ (b) $\Phi(M)$

Figure 2.4: Correlation functions ϕ and Φ of a map with 50 sources à 20 events on isotropic background (50, 000 events altogether). Also, the correlation functions of pure background maps (50, 000 events) are shown.

In figure 2.5 the influence of the number of sources and source events is shown for the case that sources may not be located on top of each other. As expected, the method is sensitive to the number of events per source and moreover, in opposite to the ring background method, it is sensitive to the number of sources, even if they do not overlap (compare 2.5 to 2.2). If the sources are not constrained to a minimum distance from each other, the event correlation method performs comparable to the ring background method (compare 2.6 to 2.3).

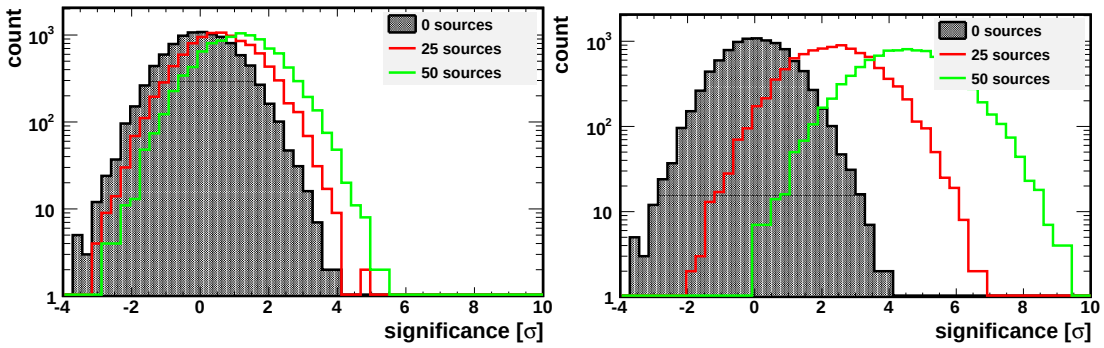

(a) $n_{src.ev} = 20$ (b) $n_{src.ev} = 40$

Figure 2.5: Event correlation method: significances for maps with and without sources obtained by normalizing in such a way that the distribution of $\Phi(M_0^i, 0.1^\circ)$ has $\mu = 0$ and $\sigma = 1$. Minimum distance between two sources is 0.2°. The number of events (source events plus background) is $50,000$.

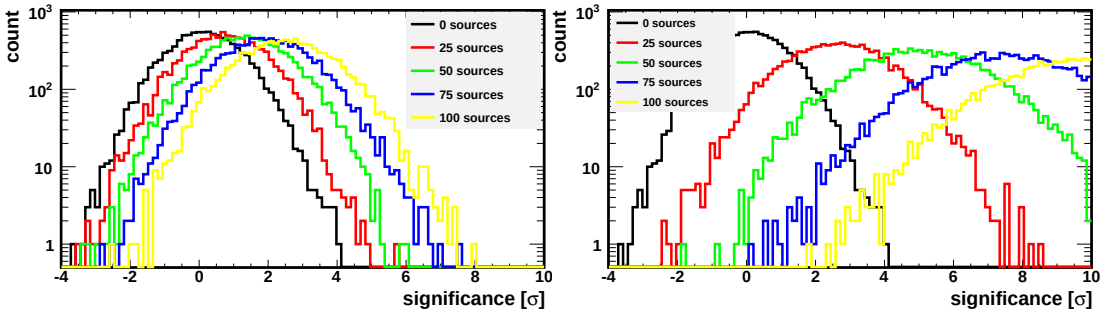

(a) $n_{src.ev} = 20$ (b) $n_{src.ev} = 40$

Figure 2.6: Event correlation method: significances for maps with and without sources obtained by normalizing in such a way that the distribution of $\Phi(M_0^i, 0.1^\circ)$ has $\mu = 0$ and $\sigma = 1$. No minimum distance between two sources is required $\Rightarrow$ sources may overlap. The number of events (source events plus background) is $50,000$.

2.3 Comparison

Detection error measure

Because the ring background method returns a significance of a signal for a position on a map whereas the event correlation method returns a significance for the signals at all positions on a map, it is difficult to compare the two methods directly. To circumvent it, an approximation of the type 1 and 2 errors is calculated. Let

- M_0^i be a set of m maps containing background only (H_0 or null hypothesis maps),
- M_1^j a set of n maps containing background and sources (H_1 or alternative hypothesis maps) and
- $F(M)$ the function that returns the signal in map M (max. significance for the ring background method and $\Phi(0.1)$ for the event correlation).

Then the overlap E of the histograms of $F(M_0^i)$ and $F(M_1^j)$ is the normalized sum of all cases where $F(M_0^i) \geq F(M_1^j)$:

$$E = \frac{1}{m\,n} \sum_{i=1}^{m} \sum_{j=1}^{n} F(M_0^i) \geq F(M_1^j) \tag{2.7}$$

The more signal is detected in the M_1^j, the more $F(M_1^j)$ is shifted to the right, the less the histograms of $F(M_0^i)$ and $F(M_1^j)$ overlap and the smaller E gets. Now, if a description on how to generate M_0^i and M_1^j is given, the performance of a method can be parametrized by only one number.

Generation of simplicistic H_0 and H_1 maps

In order to emphasize the methods' characteristics and prevent side effects of complex models, in this chapter the following simplicistic model is assumed for the generation of maps:

- sources are isotropically distributed over the map
- sources must be at least $2\,\sigma_{\text{psf}}$ away from the border
- a constant number of events per source is randomly distributed around each source, following the distance distribution $p(r) = \frac{1}{\sqrt{2\pi}\sigma} \mathrm{e}^{-\frac{r^2}{2\,\sigma^2}}$
- background events are isotropically distributed over the map (isotropic exposure)
- the sum of events is the same in all maps

Technical Issues

If the on-region of the ring gets too small, low statistics can lead to large fluctuations of the Li-Ma-significance. That happens near the border of the map (see Figure 2.1, where the size of the on-region may be reduced down to half the original size. Therefore, the significances of all bins, whose distance to the border is less than the radius of the on-region, are ignored.
To ensure equal conditions for both methods and because similar problems may also occur during the event correlation, all events which lie within the border region may only passively contribute to the correlation function, which means that a distance *to* them may be counted, but not a distance *from* them. That means that at least one of the two events must not lie within the border region.

Results

Here, the event correlation method is compared to the ring background method by measuring the overlap E. Figure 2.7 shows that if sources may not overlap, the event correlation method can benefit from an increased number of sources, while the ring background method cannot. For example, when using the event correlation method, only 12% of the maps with 40 sources à 30 source events are not detected as maps containing sources, while with the ring background method, 24% are not detected as maps containing sources.
If sources may overlap, the ring performs better and is comparable to the event correlation method (see figure 2.8). As the ring background method could not detect anything in the H.E.S.S. data, this plot also gives an idea of the upper limit of weak sources in the Galactic Centre region.

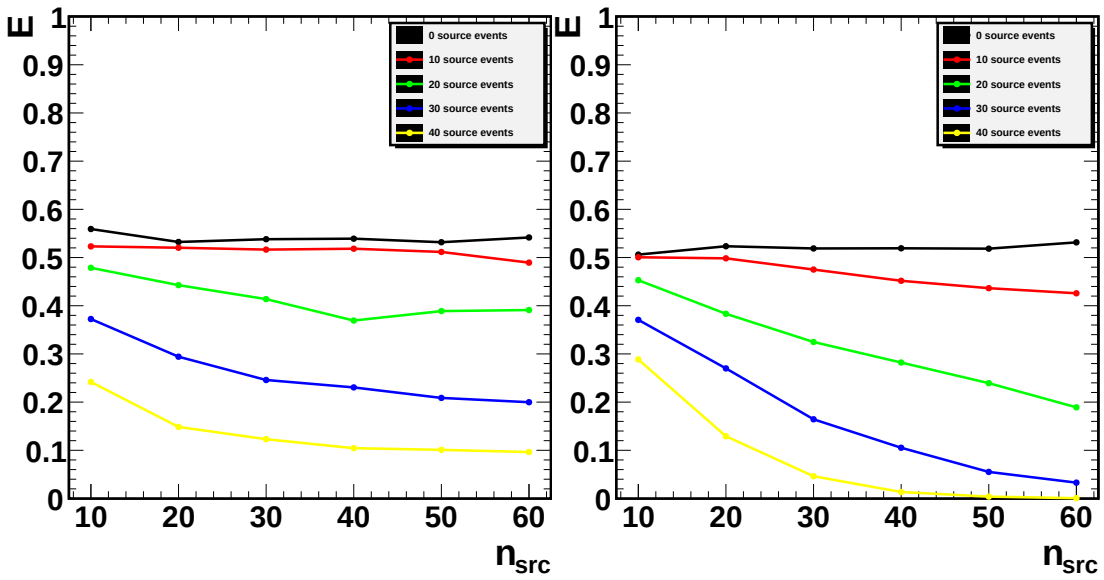

(a) Ring background (b) Event correlation

Figure 2.7: Comparison for different numbers of sources and source events on isotropic background, $50,000$ events total. Minimum distance between two sources is $0.2°$.

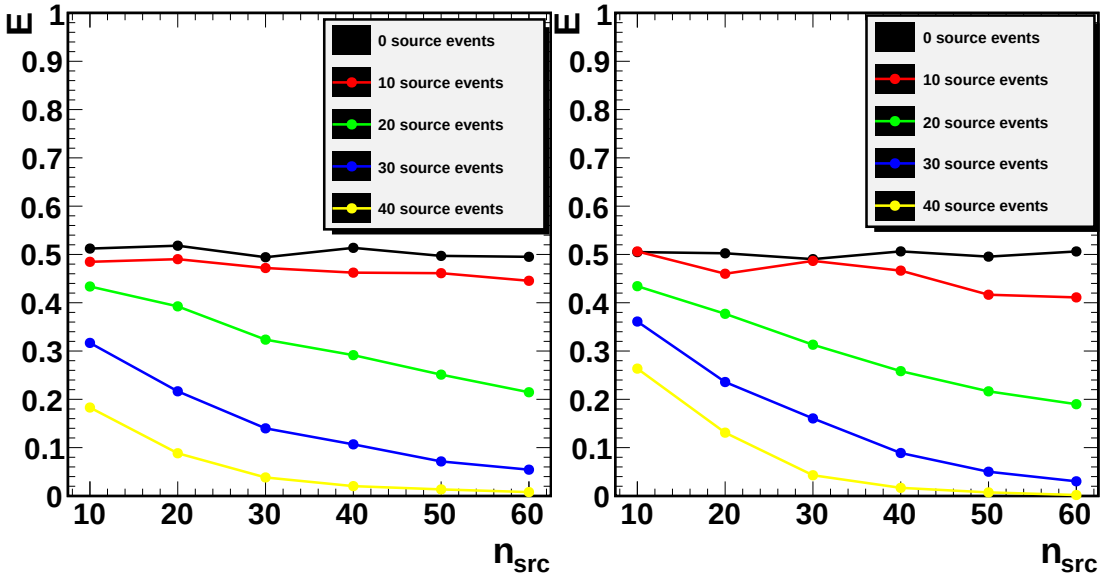

(a) Ring background (b) Event correlation

Figure 2.8: Comparison for different numbers of sources and source events on isotropic background, $50,000$ events total. No minimum distance between two sources is required $\Rightarrow$ sources may overlap.

3 Analyzing H.E.S.S. data from the Galactic Centre

In this chapter, the distribution of the γ-ray event candidates from the Galactic Centre is examined with respect to small-scale anisotropies by applying the event correlation method.
At first, several ways of generating H_0 maps that randomizes the small-scale structures of the data are investigated and it is verified that the randomization of pure background maps does not affect the correlation function. Artificial maps that feature similar large-scale distributions as the data are therefore created and analyzed.
Then, these maps with source populations distributed on them are analyzed in order to learn about the number and strengths of sources necessary for a detection.
To prevent a detection due to the already known two strong point sources, all events in a small circle around them are excluded from the analysis. Also the large-scale distributions, which are caused by varying exposure time of the telescope and diffuse emission from the molecular cloud, could lead to false detections and are therefore included into the background model.
The region of interest is a rectangle of size $4° \times 2°$ around the Galactic Centre (see figure 3.1), because it contains most of the diffuse emission (see figure 1.2). To prevent border effects during the analysis, the map is extended in every direction.

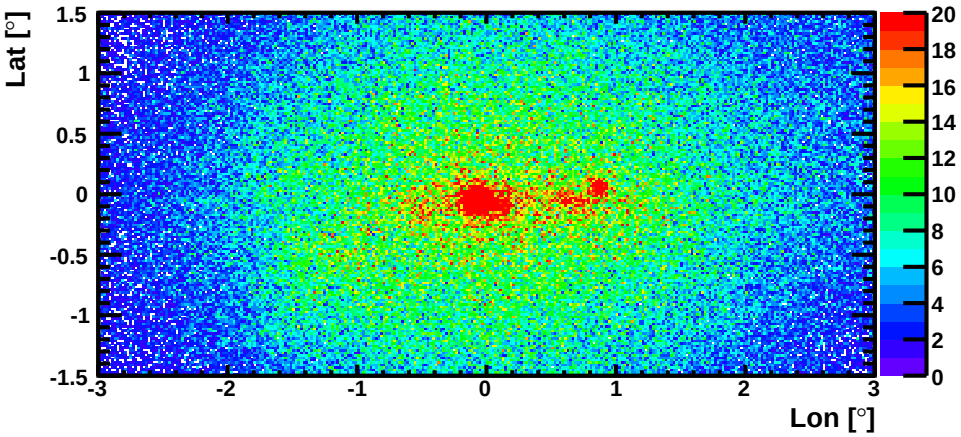

Figure 3.1: binned event map of the region of interest, bin width: 0.02°

3.1 Generation of H_0 maps

H_0 maps can be generated based on a model of the large-scale distributions or by scattering the H_1 map. To verify that a generated H_0 map M_0 has approximately the same large-scale structure as the H_1 map M_1, the difference between M_0 and a smoothed version of M_1 is estimated by calculating the mean squared error of their binned versions:

$$\mathrm{MSE}(M_0, G_\sigma(M_1)) \,,$$

with the mean squared error defined as

$$\mathrm{MSE}(A, B) = \frac{1}{n}\sum_{k=0}^{n}(A_k - B_k)^2 \,,$$

for two maps A and B containing n bins each. G denotes the Gaussian smoothing operator of width σ, which should not be larger than σ_{psf}, because otherwise, also the large-scale structures are destroyed. A good compromise between destructing small-scale structures and preserving large-scale structures can be found by comparing $G_\sigma(H_1)$ (see figure 3.2) to the exposure map and the molecular cloud (see figure 3.7 (a) and (b)). Now, assuming that the MSE is an adequate measure for the estimation of the structural similarity, if

$$\mathrm{MSE}(M_0^i, G_\sigma(M_1) \quad \leq \quad \mathrm{MSE}(M_1, G_\sigma(M_1))$$

for several H_0 maps M_0^i and the H_1 map M_1, the model is regarded as suitable. In order to find the best parameter (set) for a method generating H_0 maps, the distribution of $\mathrm{MSE}(M_0^i, G_\sigma(M_1))$ is compared to $\mathrm{MSE}(M_1, G_\sigma(M_1))$ by calculating the difference

$$d = \mathrm{MSE}(M_1, G_\sigma(M_1)) - \frac{1}{m}\sum_{i=0}^{m}\mathrm{MSE}(M_0^i, G_\sigma(M_1)) \,,$$

which measures how much more similar the M_0^i are to $G_\sigma(M_1)$ than M_1 is. Normalizing the $\mathrm{MSE}(M_0^i, G_\sigma(M_1))$ to $\mu = 0$ and $\sigma = 1$ turns all MSEs into significances, which makes it easy to compare among different G_σ. In the following, all MSEs will be normalized MSEs (depending on H_0) and thus,

$$d = \mathrm{MSE}(M_1, G_\sigma(M_1)) \,.$$

Note that all errors are first calculated after having excluded the two strong point sources.

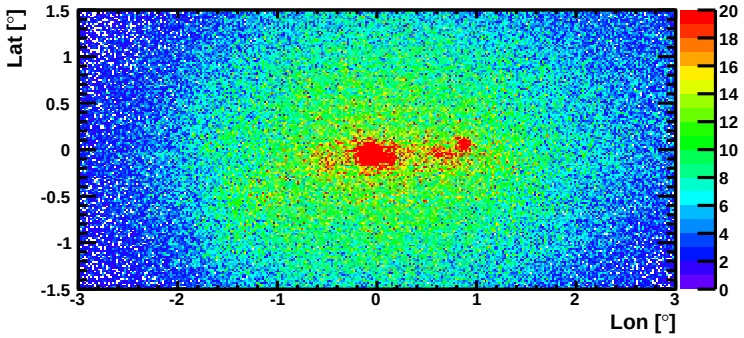

(a) M_1

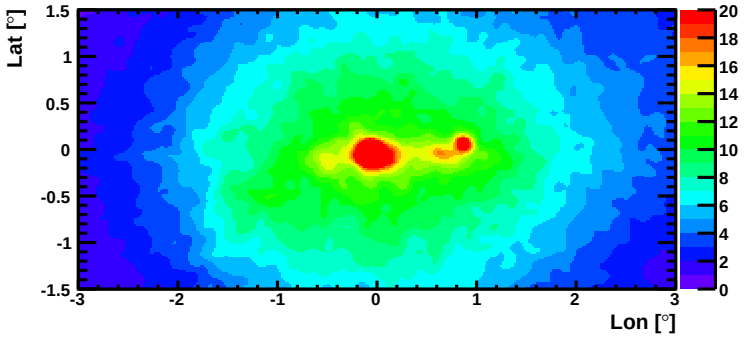

(b) $G_{\sigma=0.05^\circ}(M_1)$

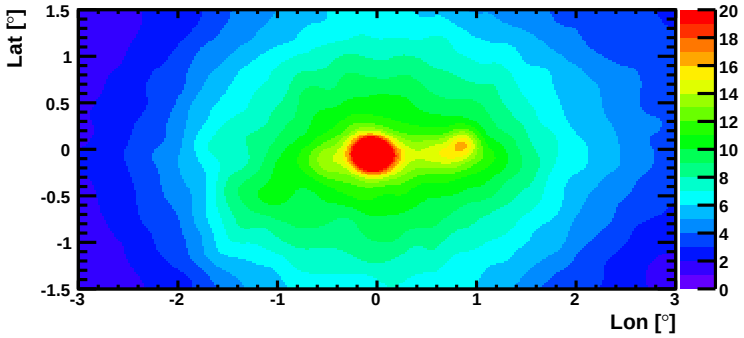

(c) $G_{\sigma=0.10^\circ}(M_1)$

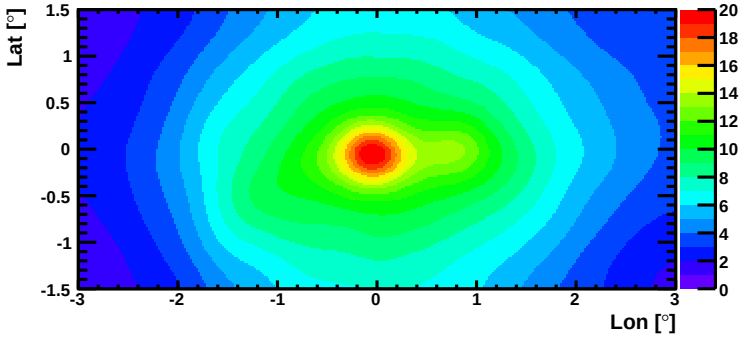

(d) $G_{\sigma=0.20^\circ}(M_1)$

Figure 3.2: H_1 map smoothed by G_σ

3.1.1 Scattering the H_1 map in longitude and latitude

Given M_1, a scattered version

$$M_0 = S_{\sigma_S}(M_1)$$

is obtained by translating each event x_i by a random vector sampled from a 2D Gaussian distribution of width σ_S:

$$x_i^{\text{new}} = x_i + g_\sigma$$

This procedure applies to *all* events in the data set, not only to those inside of the region of interest. Otherwise, events get scattered out of the region of interest without any outside events being scattered into it, which would lead to low densities at the borders. For the same reason, exclusion regions are used only after the scattering.

Figure 3.3 shows examples of H_0 maps obtained for different S_{σ_S}, whose large-scale structures are compared to the large-scale structures of M_1, assuming that $G_{0.1^\circ}$ models these structures well. The distributions of the normalized ($\mu = 0$, $\sigma = 1$) mean squared errors of $S_{\sigma_S}(M_1)$ along with the mean squared error of the H_1 map (blue mark) are also shown.
If most of the H_0 maps are more similar to the smoothed H_1 map than the H_1 map is (blue mark ≥ 0), the model is probably not too inaccurate.

After having chosen a σ_G, the differences d for different S_{σ_S} are calculated and shown in figure 3.3.
With σ_S starting from 0, the small-scale structures of M_1 are increasingly destroyed, making $S_{\sigma_S}(M_1)$ more and more similar to $G_{\sigma_G}(M_1)$, until events start getting scattered so heavily that even the large-scale structures are destroyed and events are scattered out of the exclusion regions.
So the best σ_S is where d is maximal because then, the small structures of M_1 are destroyed and it is closest to the smoothed M_1.

3.1.2 Scattering the H_1 map in longitude

Because the diffuse emission is extended mainly in longitude, scattering too much in latitude would result in H_0 maps not having a structure which is present in the H_1 map. The operator T_{σ_T} generates H_0 maps

$$M_0 = T_{\sigma_T}(M_1)\,.$$

by translating each event x_i in longitude, by a random distance sampled from a 1D Gaussian distribution:

$$x_i^{\text{new}} = x_i + g_{\sigma_T}$$

Figure 3.4 shows H_1 scattered in longitude by T_{σ_T} along with the plots of the mean squared errors.

3.1.3 Sampling from smoothed data

When events are scattered, they might be scattered out of the exclusion region and create higher event densities there, which might lead to false detections. If the H_1 map is smoothed by σ_U (such that large-scale structures still remain) and then interpreted as a probability distribution, event positions can be sampled from it and the generated H_0 maps have exactly as many events as the H_1 map. The operator U generates H_0 maps in such a way:

$$M_0 = U_{\sigma_U}(M_1)\,.$$

Example H_0 maps sampled from $G_{\sigma_G}(M_1)$ with the corresponding histograms for d along with the graph for $d(\sigma_G)$ are shown in figure 3.5. Although with this randomization method events are not scattered out of the exclusion regions, there are high event densities around the exclusion regions anyway, because during the smoothing the events of the exclusion regions are smeared out and then new events are sampled from that distribution (see the ring with higher event density around the left exclusion region in figure 3.5 (b)).

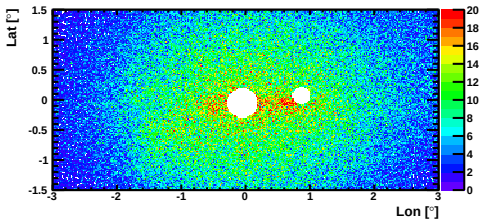

(a) M_1

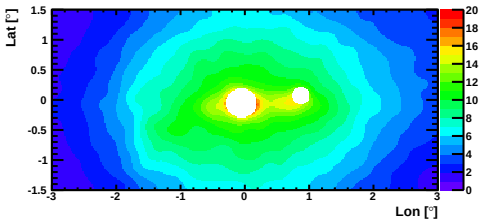

(b) $G_{0.1^\circ}(M_1)$

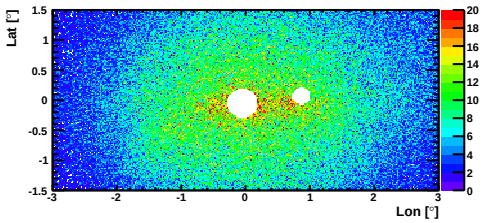

(c) example H_0 map: $S_{0.1^\circ}(M_1)$

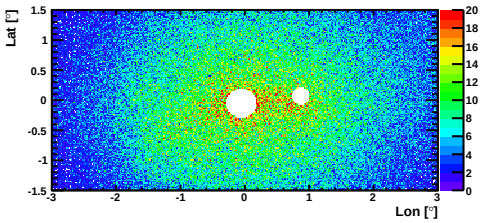

(d) example H_0 map: $S_{0.2^\circ}(M_1)$

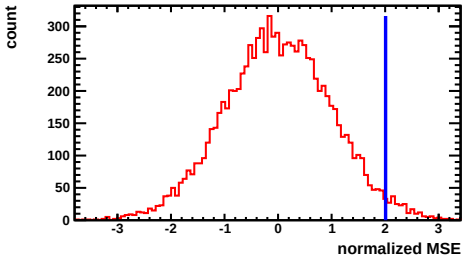

(e) distribution of normalized $\mathrm{MSE}(S_{0.1^\circ}(M_1), G_{0.1^\circ}(M_1))$ for H_0 maps and $\mathrm{MSE}(M_1, G_{0.1^\circ}(M_1))$ in blue

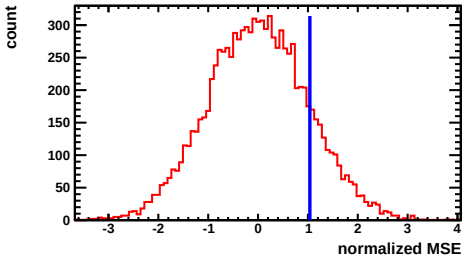

(f) distribution of normalized $\mathrm{MSE}(S_{0.2^\circ}(M_1), G_{0.1^\circ}(M_1))$ for H_0 maps and $\mathrm{MSE}(M_1, G_{0.1^\circ}(M_1))$ in blue

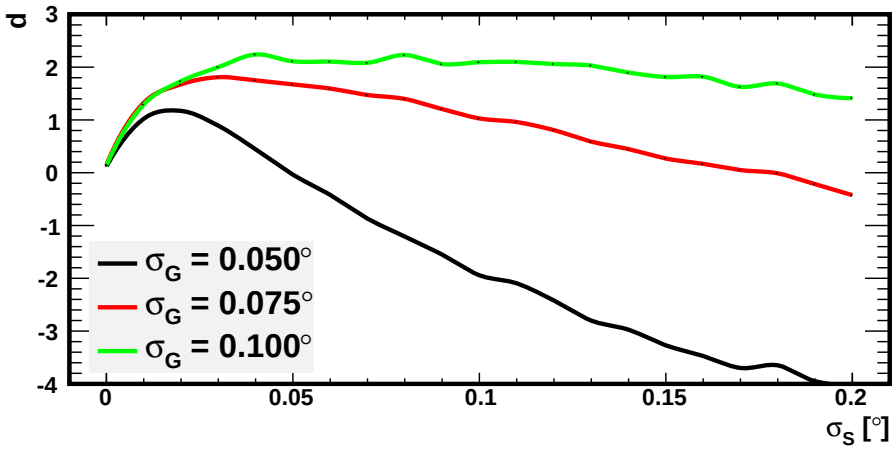

(g) normalized $\mathrm{MSE}(M_1, G_{\sigma_G}(M_1))$ for different S_{σ_S}

Figure 3.3: Scattering in longitude and latitude: $S_{0.1^\circ}(M_1)$ and $S_{0.2^\circ}(M_1)$ compared to M_1 assuming $G_{0.1^\circ}(M_1)$ models the large-scale structure of M_1 well

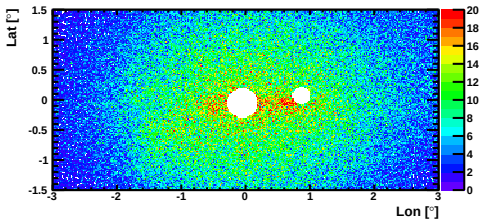

(a) M_1

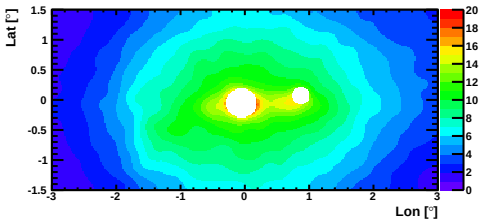

(b) $G_{0.1^\circ}(M_1)$

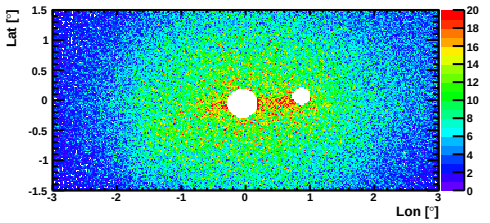

(c) example H_0 map: $T_{0.1^\circ}(M_1)$

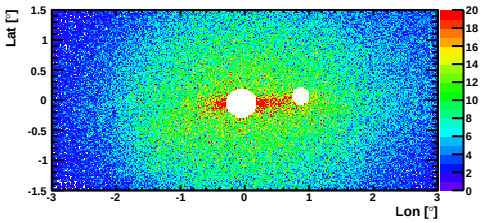

(d) example H_0 map: $T_{0.2^\circ}(M_1)$

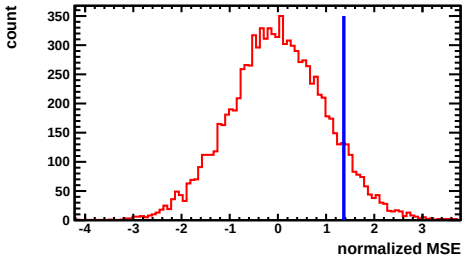

(e) distribution of normalized $\mathrm{MSE}(T_{0.1^\circ}(M_1), G_{0.1^\circ}(M_1))$ for H_0 maps and $\mathrm{MSE}(M_1, G_{0.1^\circ}(M_1))$ in blue

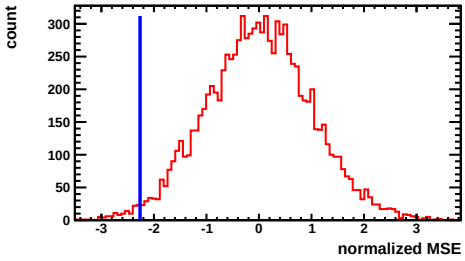

(f) distribution of normalized $\mathrm{MSE}(T_{0.2^\circ}(M_1), G_{0.1^\circ}(M_1))$ for H_0 maps and $\mathrm{MSE}(M_1, G_{0.1^\circ}(M_1))$ in blue

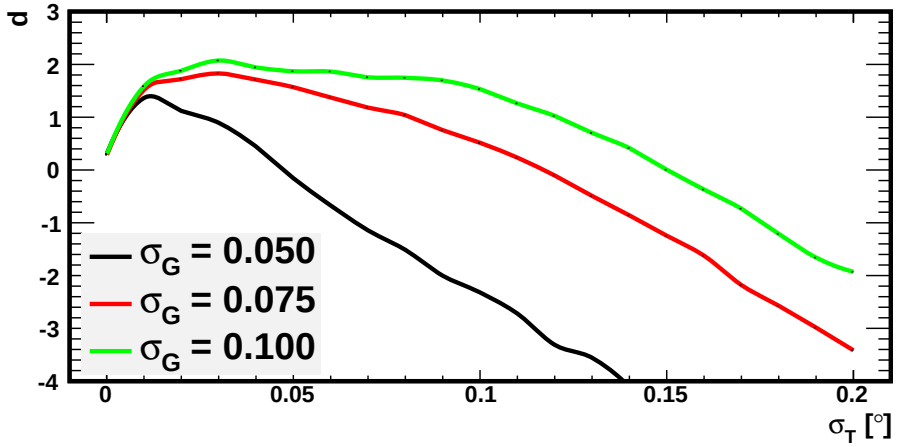

(g) normalized $\mathrm{MSE}(M_1, G_{\sigma_G}(M_1))$ for different T_{σ_T}

Figure 3.4: Scattering in longitude: $T_{0.1^\circ}(M_1)$ and $T_{0.2^\circ}(M_1)$ compared to M_1 for $G_{0.1^\circ}(M_1)$

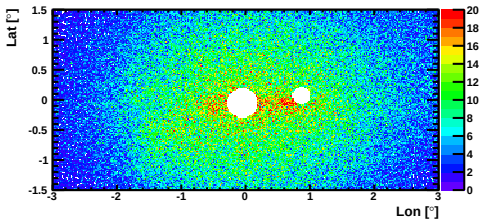

(a) M_1

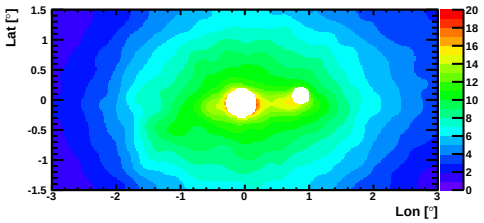

(b) $G_{0.1^\circ}(M_1)$

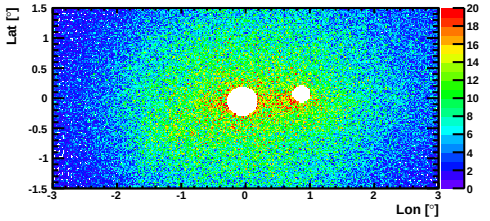

(c) example H_0 map: $U_{0.1^\circ}(M_1)$

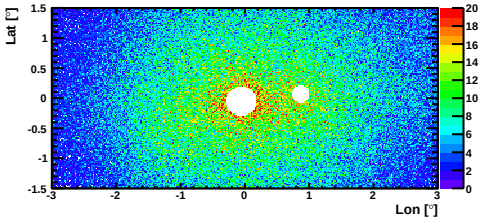

(d) example H_0 map: $U_{0.2^\circ}(M_1)$

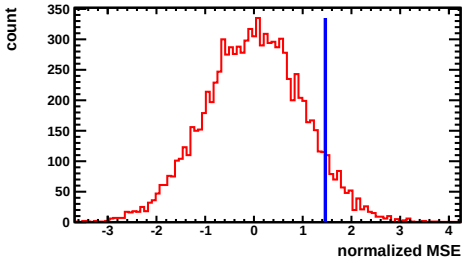

(e) distribution of normalized MSE$(U_{0.1^\circ}(M_1), G_{0.1^\circ}(M_1))$ for H_0 maps and MSE$(M_1, G_{0.1^\circ}(M_1))$ in blue

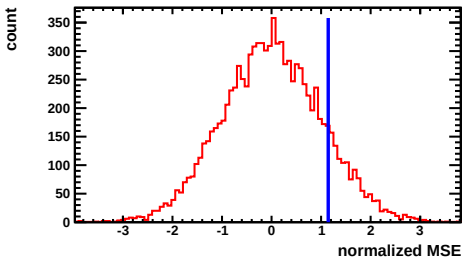

(f) distribution of normalized MSE$(U_{0.2^\circ}(M_1), G_{0.1^\circ}(M_1))$ for H_0 maps and MSE$(M_1, G_{0.1^\circ}(M_1))$ in blue

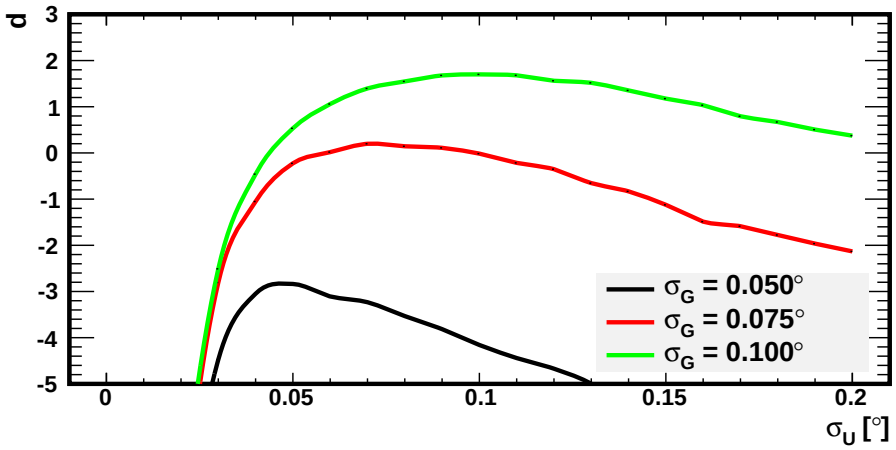

(g) normalized MSE$(M_1, G_{\sigma_G}(M_1))$ for different U_{σ_U}

Figure 3.5: Sampling from the smoothed H_1 map: $U_{0.1^\circ}(M_1)$ and $U_{0.2^\circ}(M_1)$ compared to M_1 for $G_{0.1^\circ}(M_1)$

3.2 Verification of the randomization algorithms

This section investigates in Monte Carlo simulations if the generated H_0 maps are valid by comparing artificial maps without sources to the H_0 maps generated from them. If new structures that affect the result of the event correlation function are introduced or removed, this effect must be considered.

3.2.1 Artificial maps

The artificial maps have to be very similar to the data and are therefore generated according to the known large-scale event distributions:

- 270.000 events are distributed according to the exposure map (see figure 3.6 (a)).
- 5000 events are distributed according to the density of the molecular cloud (see figure 3.6 (b)).
- Sagittarius A* and G 0.9+0.1 are simulated by adding two point-sources at their positions with 4000 and 1500 events, respectively (see figure 3.6 (c)).

Figure 3.7 then shows an example of a final artificial map next to the data for comparison.

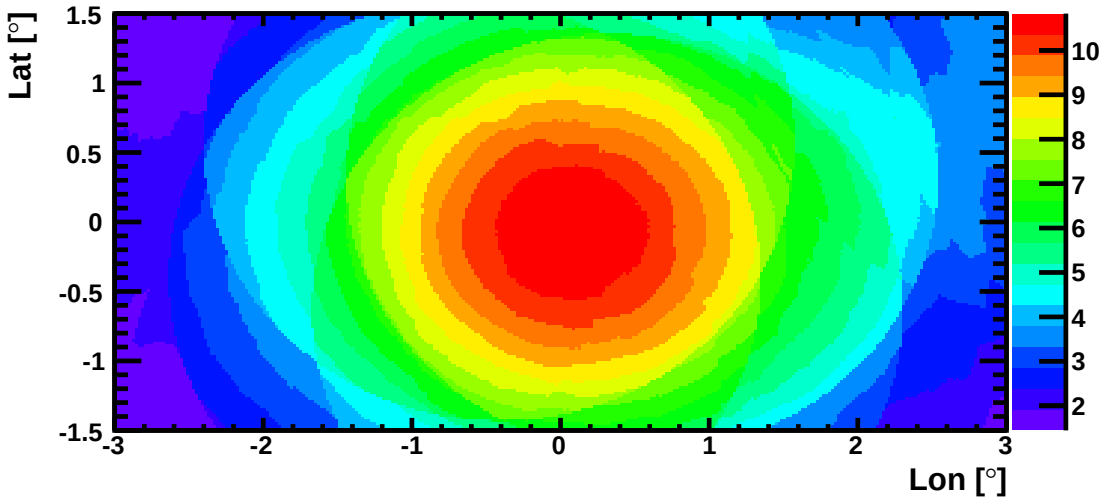

(a) exposure map

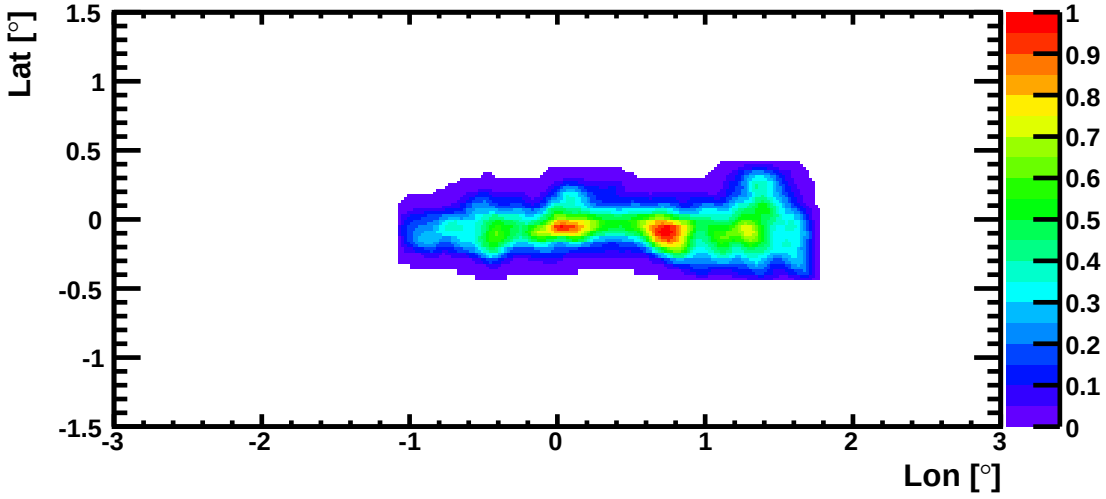

(b) densities of the molecular cloud

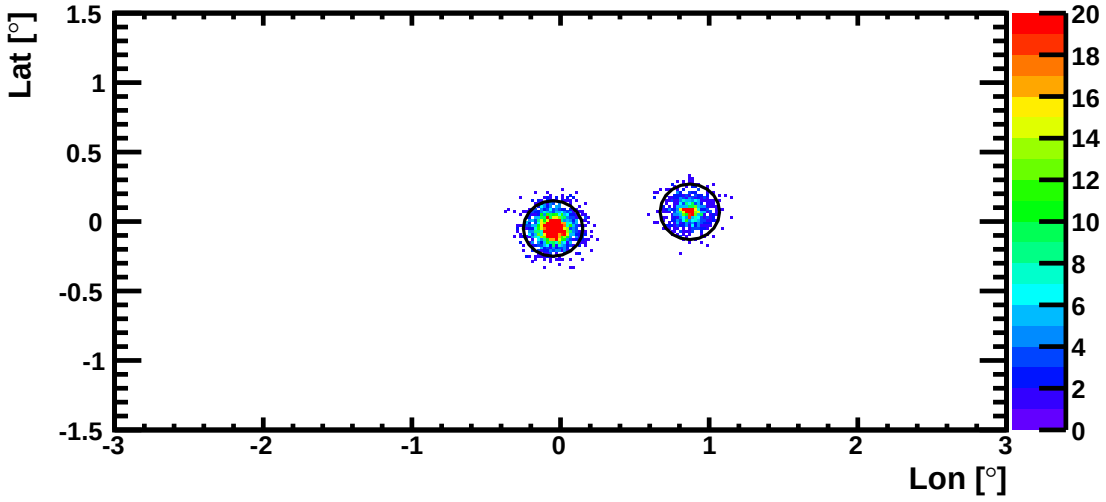

(c) two strong point sources

Figure 3.6: Components of an artificial map without sources

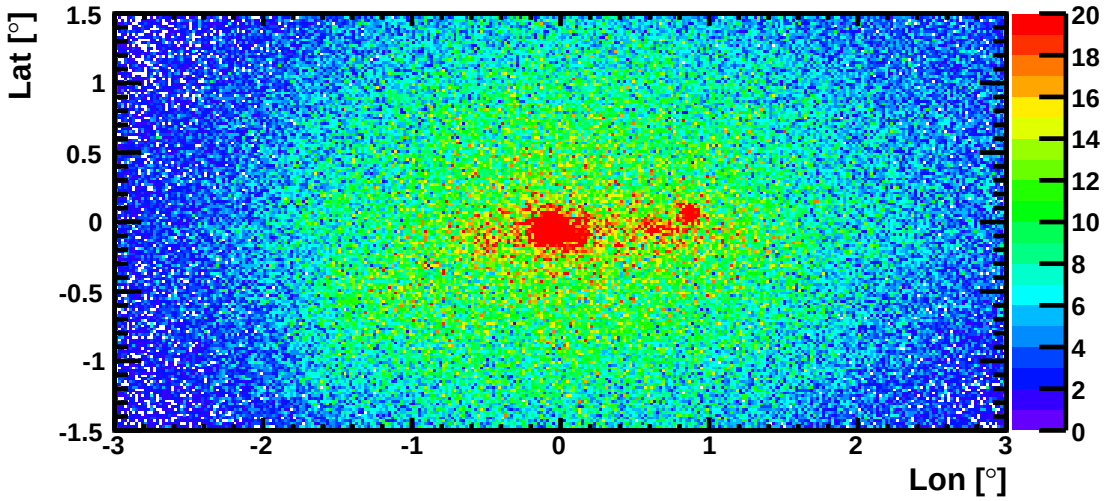

(a) data

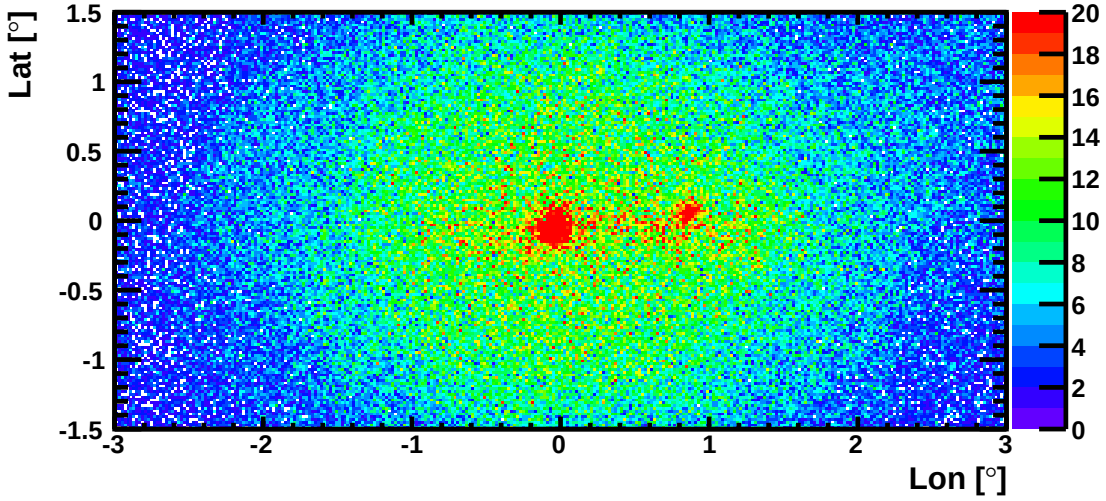

(b) artificial event map

Figure 3.7: Event map generated according to the exposure map and the density of the molecular cloud, with the two strong point sources included.

3.2.2 H_1 maps without sources compared to their H_0 maps

The values of the correlation functions at 0.1° before (M_1) and after randomization (M_0), normalized to the mean correlation function of the randomized maps, are shown in figure 3.8. The correlation function is nearly independent of slight scattering (see (a), (b), (d) and (e)) and slight scattering in longitude performs a bit better than slight scattering in longitude and latitude (compare (b) and (e): the red curve in (e) is less shifted to the right than in (b)), because the structures caused by the diffuse emission, which are extended mostly in longitude, are not destroyed.
Strong scattering unexpectedly shifts the mean of the H_1 maps to the left (see (c) and (f)), which means that during the scattering, new structures that affect the correlation function must have been introduced to the H_0 maps. Most probably, events from the two strong point sources are scattered out of the exclusion regions (see figure 3.10). The reason for the correlation function being less prone to strong longitude-latitude scattering is that it scatters the events of the strongest point source Sagittarius A*at $(0^\circ, 0^\circ)$ nearly according to the exposure map (compare 3.10 (b) to 3.7 (a)).

Figure 3.9 shows the effect on the correlation function of randomizing maps with the above methods for the complete range of σ from 0.02° to 0.2°. It tells for a given size of an exclusion region how much the map may be randomized without affecting the correlation function.
If, for example, the radii of the exclusion regions are chosen to be $r_1 = r_2 = 0.3^\circ$, scattering in longitude and latitude may be done with σ_S up to 0.16° (see 3.9 (a)). For scattering in longitude only, the range for σ_T is similar (see 3.9 (b)). When H_0 maps are sampled from a smoothed H_1 map, all $\sigma_U < 0.08^\circ$ and $\sigma_U > 0.12^\circ$ affect the correlation function and must therefore not be chosen.
The shape of the curves suggests a superposition of effects that influence the correlation function (as mentioned above: scattering events out of the exclusion regions and destruction of large-scale structures). So to be sure, they are investigated independently.

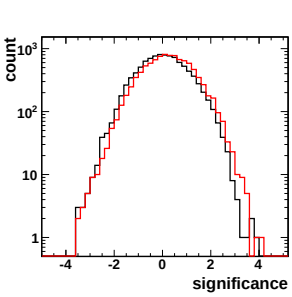

(a) $\Phi(M_1, 0.1°)$, $\Phi(S_{0.04°}(M_1), 0.1°)$

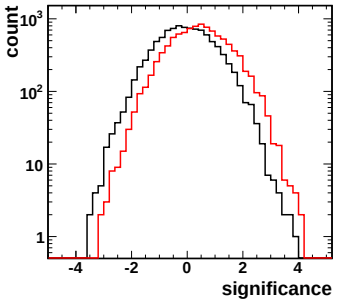

(b) $\Phi(M_1, 0.1°)$, $\Phi(S_{0.12°}(M_1), 0.1°)$

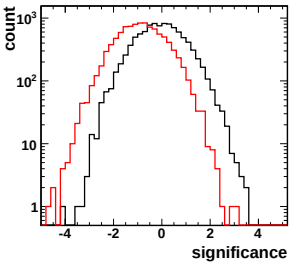

(c) $\Phi(M_1, 0.1°)$, $\Phi(S_{0.20°}(M_1), 0.1°)$

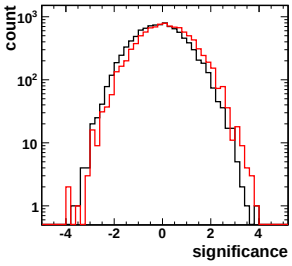

(d) $\Phi(M_1, 0.1°)$, $\Phi(T_{0.04°}(M_1), 0.1°)$

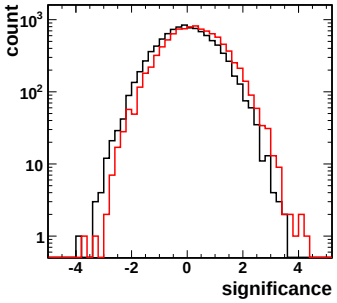

(e) $\Phi(M_1, 0.1°)$, $\Phi(T_{0.12°}(M_1), 0.1°)$

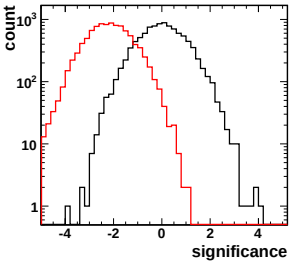

(f) $\Phi(M_1, 0.1°)$, $\Phi(T_{0.20°}(M_1), 0.1°)$

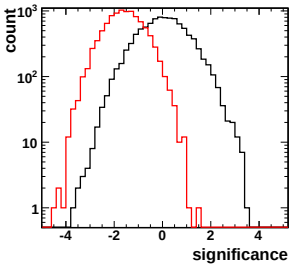

(g) $\Phi(M_1, 0.1°)$, $\Phi(U_{0.04°}(M_1), 0.1°)$

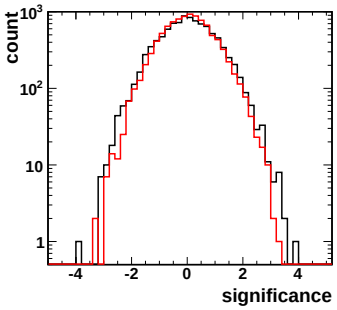

(h) $\Phi(M_1, 0.1°)$, $\Phi(U_{0.12°}(M_1), 0.1°)$

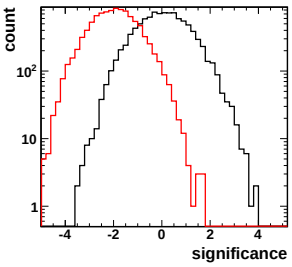

(i) $\Phi(M_1, 0.1°)$, $\Phi(U_{0.20°}(M_1), 0.1°)$

Figure 3.8: Effect of randomization methods on the correlation function for H_1 maps without sources (red) compared to the corresponding H_0 maps created from them (black), depending on randomization. The values of the correlation functions at 0.1° are histogrammed after normalization to $\mu = 0$ and $\sigma = 1$ for H_0 maps, thus yielding significances. Exclusion radii are $r_1 = r_2 = 0.3°$.

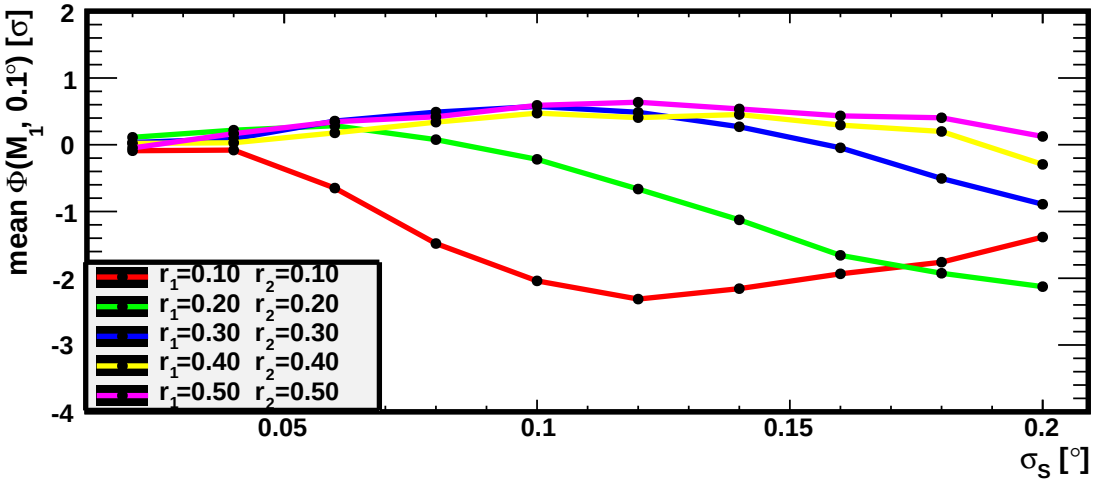

(a) scattered in longitude and latitude

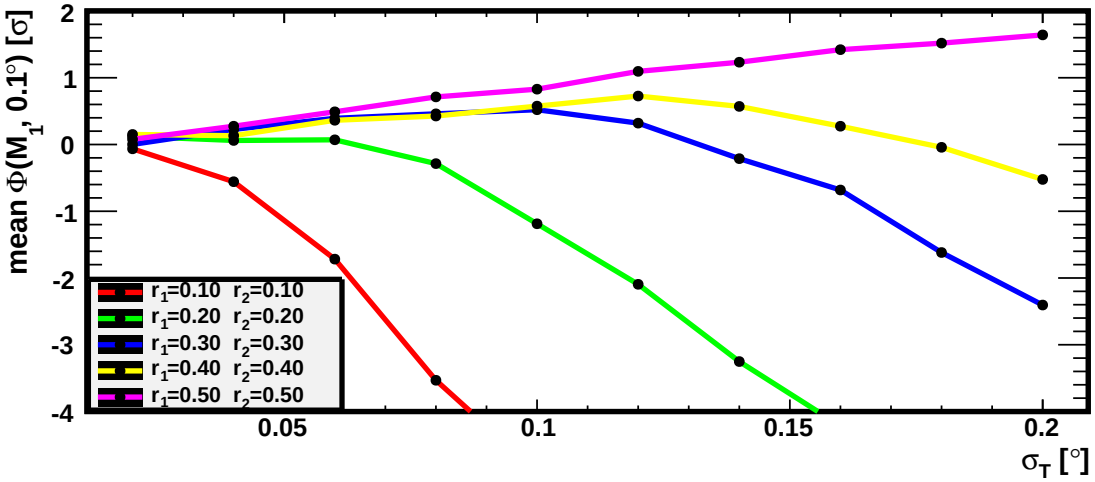

(b) scattered in longitude

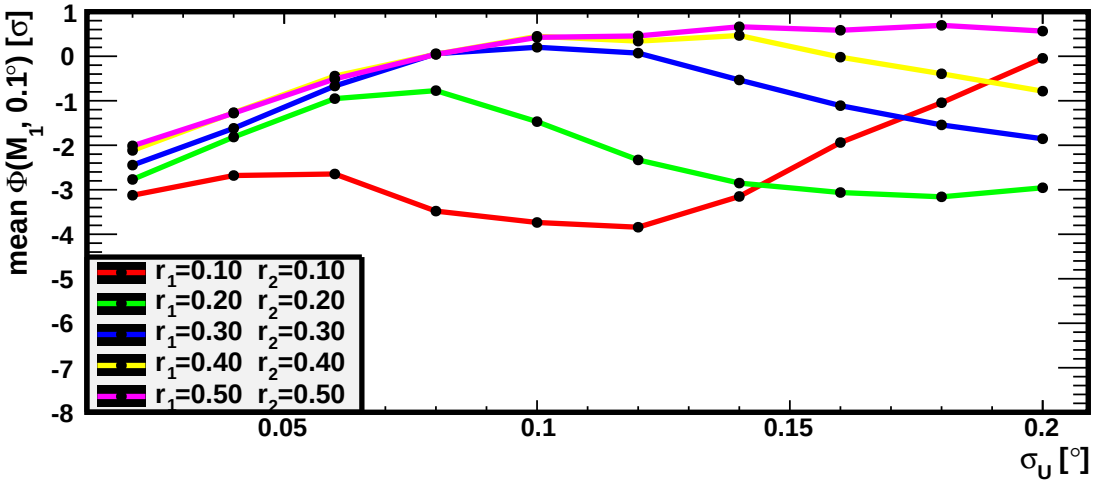

(c) sampled from smoothed map

Figure 3.9: Shift of the mean correlation function (significance) of artificial H_1 maps **with background modeled according to the large-scale distributions also present in the data** without a population of weak sources depending on randomization for different exclusion radii

3.2.3 Influence of exclusion regions

To investigate the influence of the size of the exclusion regions, the events of the two strong point sources are counted that land outside of the exclusion regions after randomization (see figure 3.10 and 3.11). The influence on the correlation function is shown in figure 3.12, where these two sources are placed on an isotropic background in order to eliminate effects caused by a complex background model and to focus on the effects of these point sources and their exclusion regions only. For the two strong point sources used in the simulations, a good compromise are exclusion regions with radii of $r_1 = r_2 = 0.3°$ and $\sigma < 0.1°$.

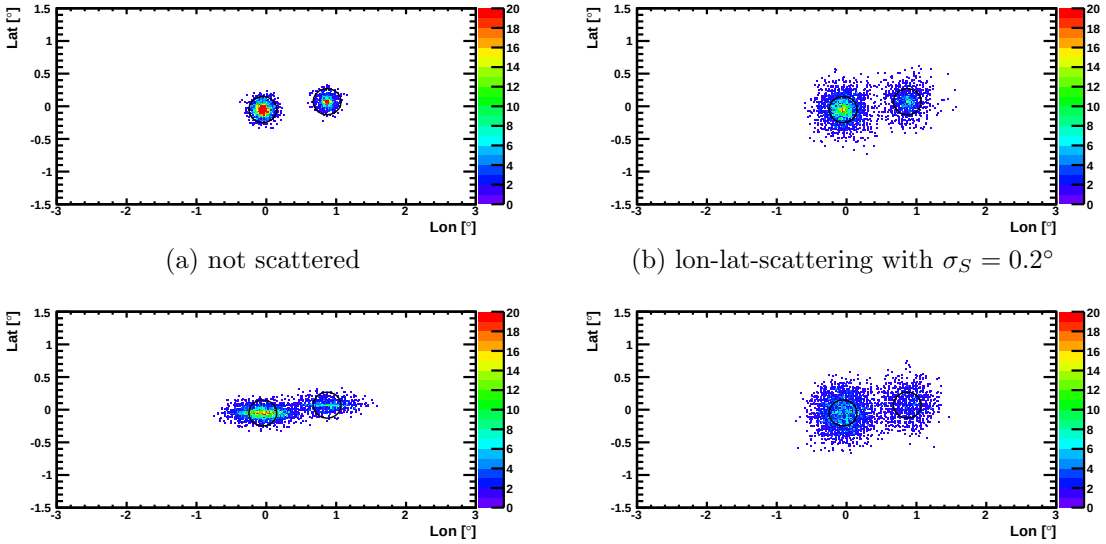

(a) not scattered

(b) lon-lat-scattering with $\sigma_S = 0.2°$

(c) lon-scattered with $\sigma_T = 0.2°$

(d) sampled from map with $\sigma_U = 0.2°$

Figure 3.10: The two strong point sources randomized by different methods. The exclusion regions are marked by black circles.

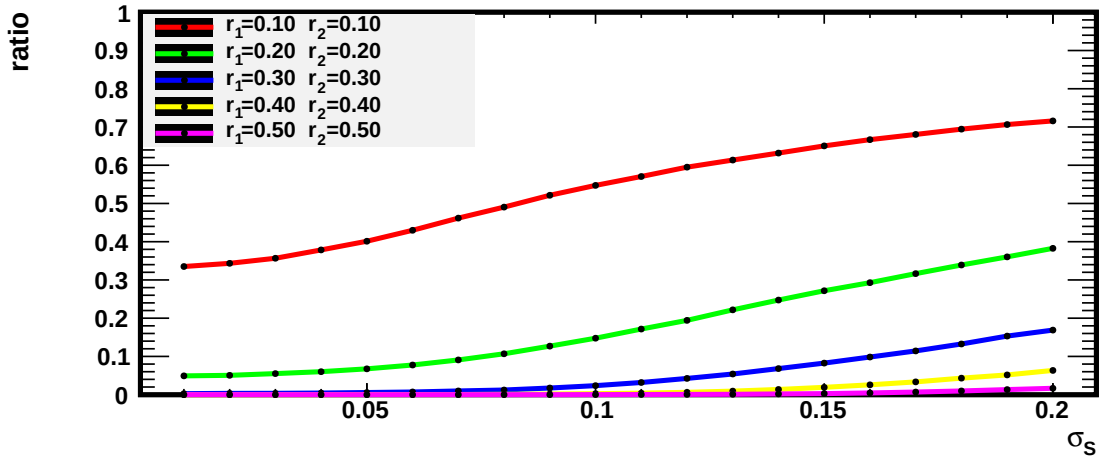

(a) scattered in longitude and latitude

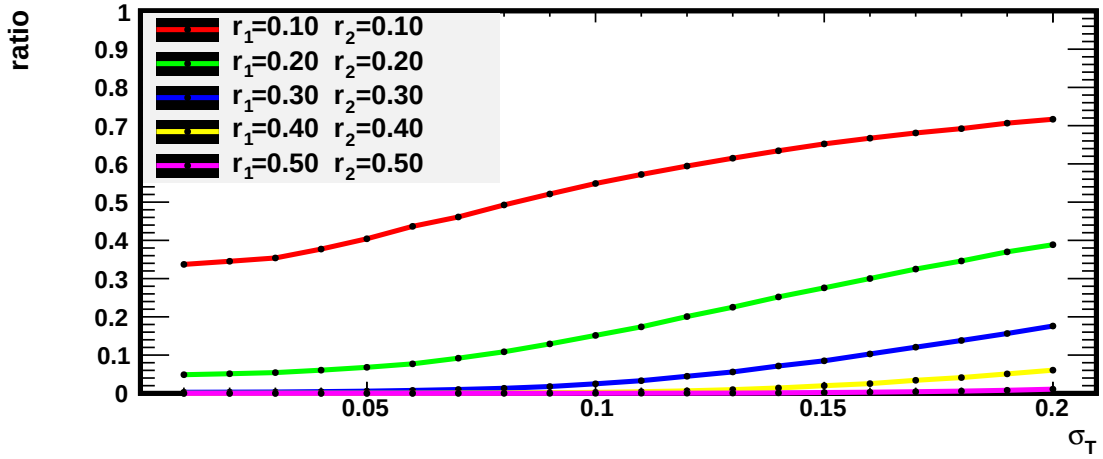

(b) scattered in longitude

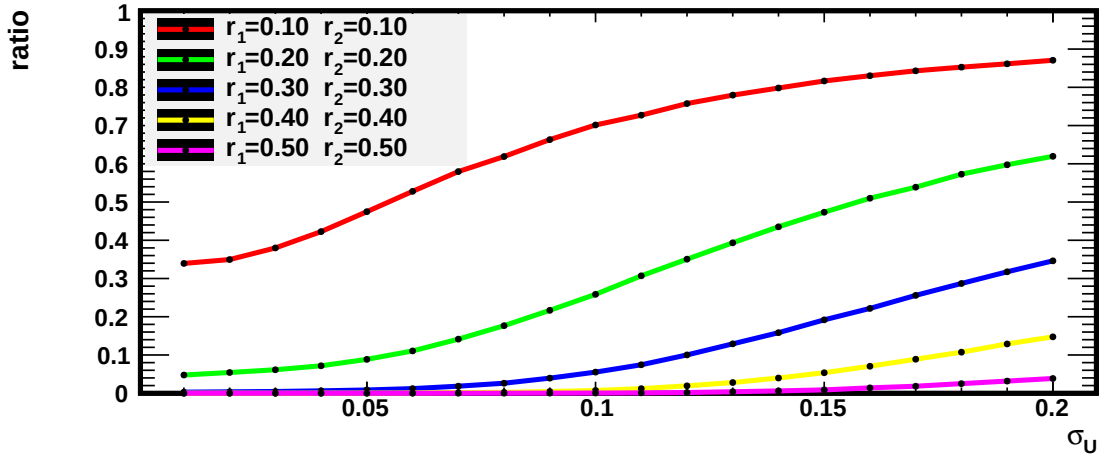

(c) sampled from smoothed map

Figure 3.11: Ratio of events outside of the exclusion region after randomizing for different radii r of the exclusion regions

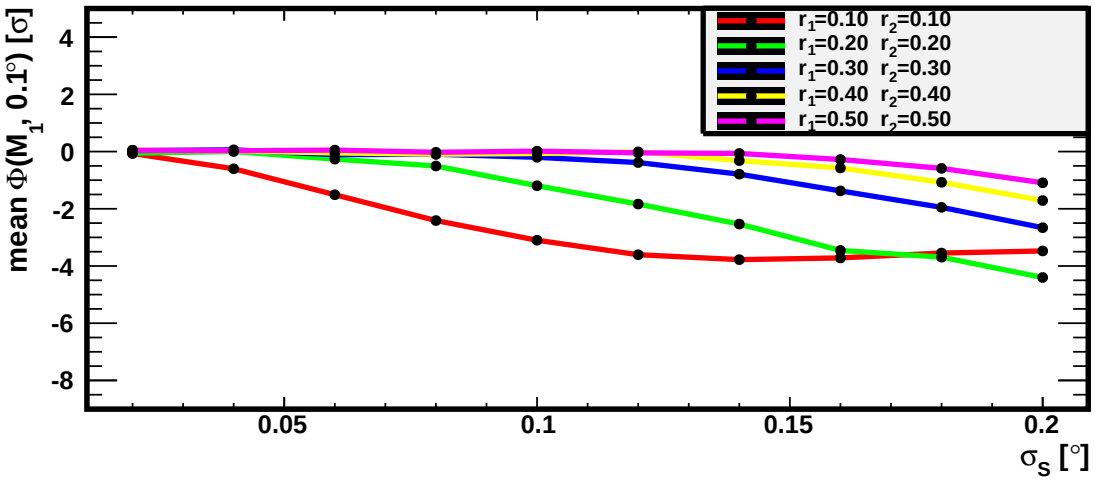

(a) scattered in longitude and latitude

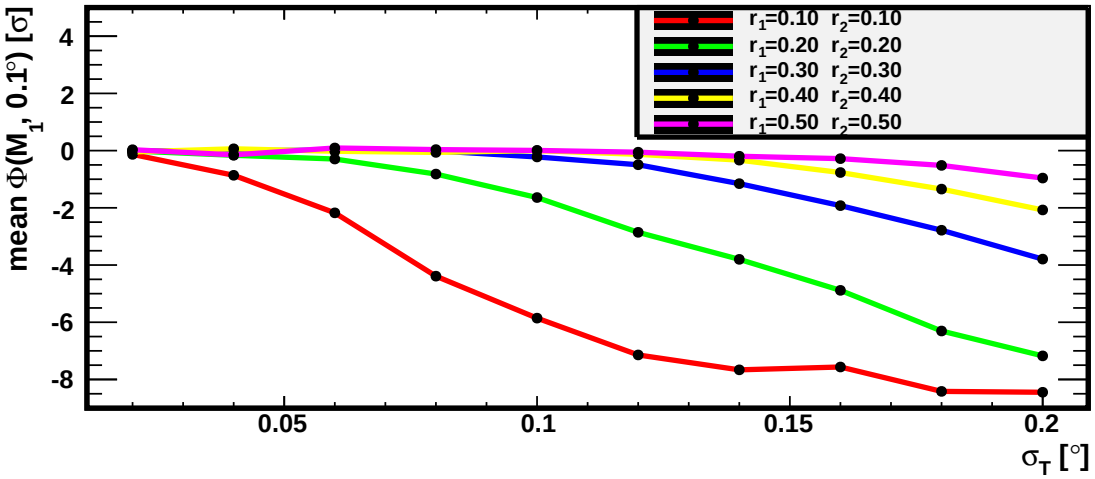

(b) scattered in longitude

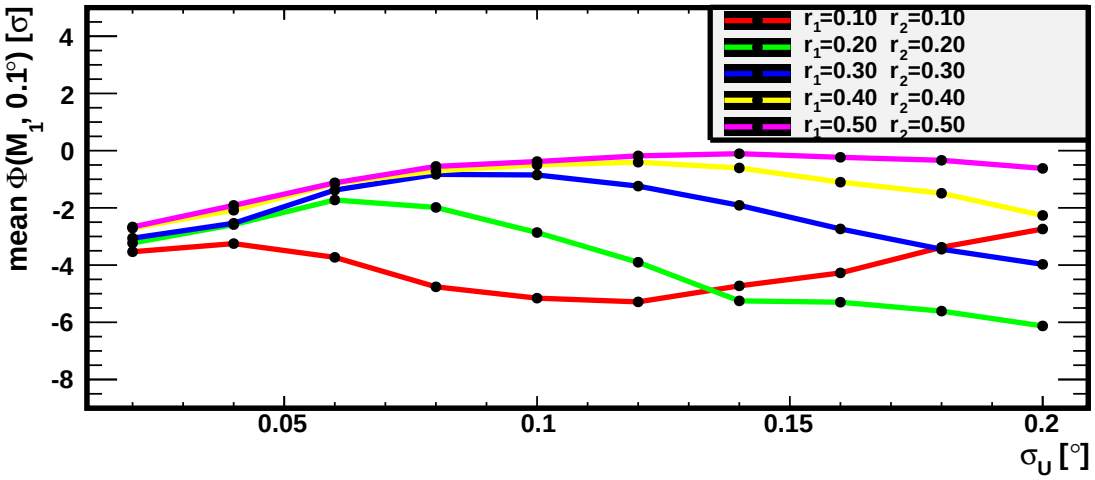

(c) sampled from smoothed map

Figure 3.12: shift of the mean correlation function (significance) at $r = 0.1°$ for maps with the two strong point sources on **isotropic background** and varying exclusion regions

3.2.4 Influence of large-scale structures

The influence of the randomization on the large-scale structures is examined by calculating the correlation functions for the same H_1 maps as before, but without the two strong point sources (see figure 3.9).

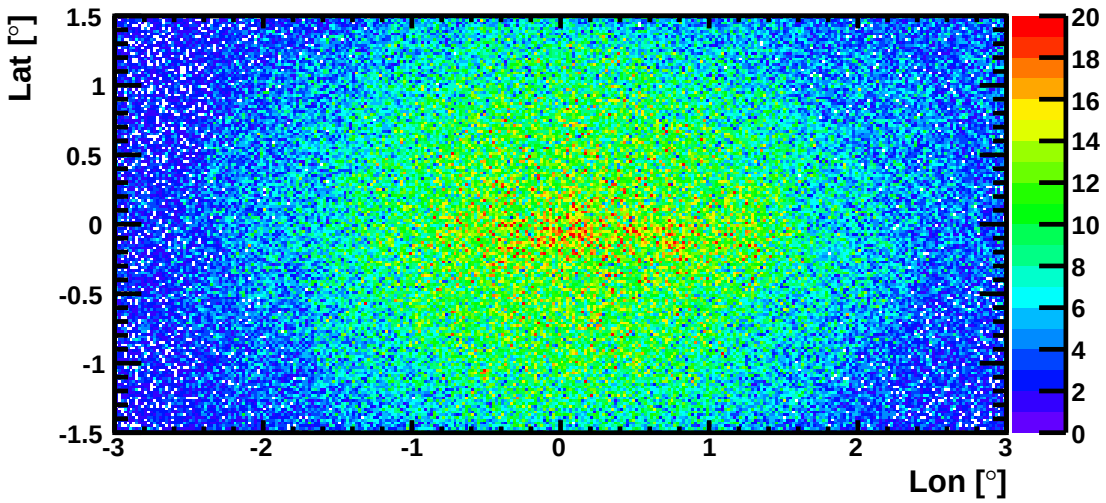

Figure 3.13: artificial H_1 map without Sagittarius A* and G 0.9+0.1

Figure 3.14 shows that already slight scattering changes the map so much that the correlation function is so heavily affected that the randomization algorithms can not be used for analysis. However, without the two strong point sources, there are neither exclusion regions and that makes the correlation function more dependent on the randomization of the map, because the area with the highest event density and strongest gradients is not masked anymore.
In the simulations, those regions are excluded, the effect becomes less problematic and the randomization methods can be used after all.

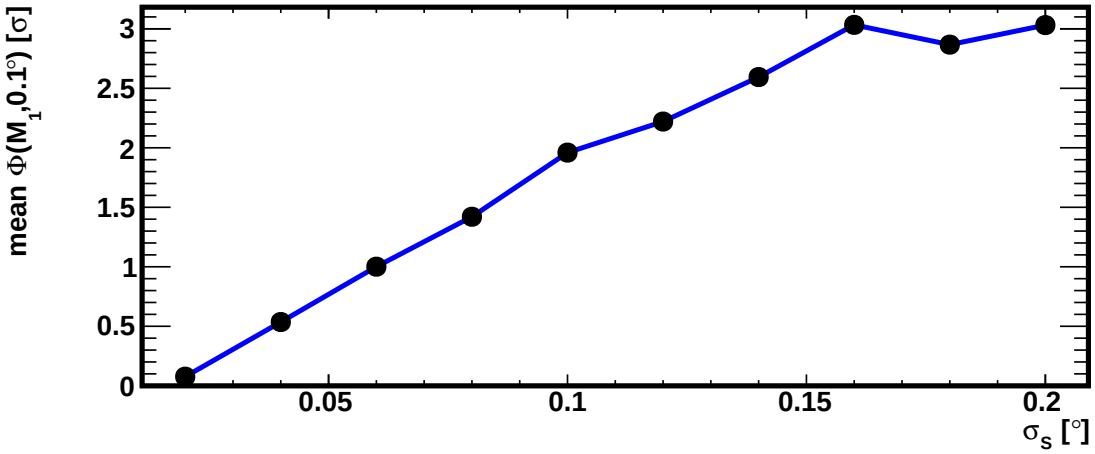

(a) scattered in longitude and latitude

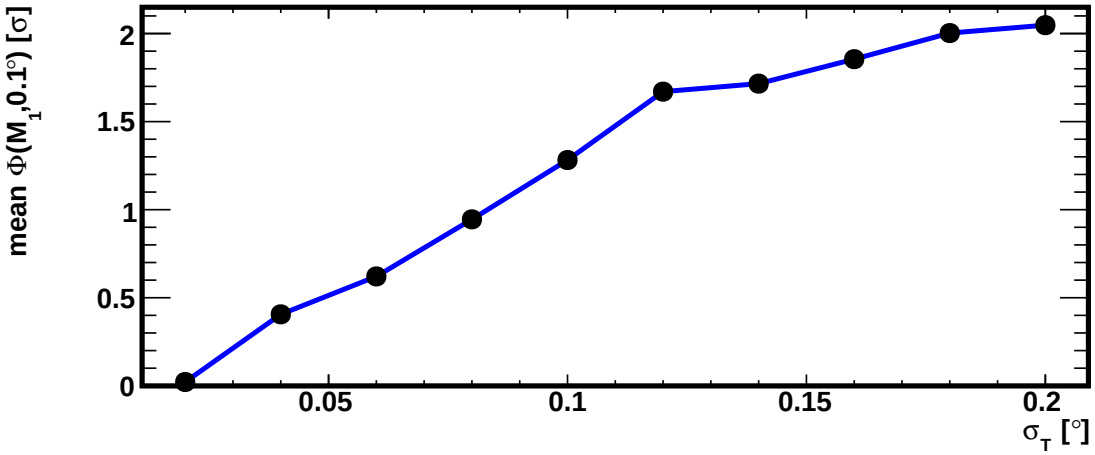

(b) scattered in longitude

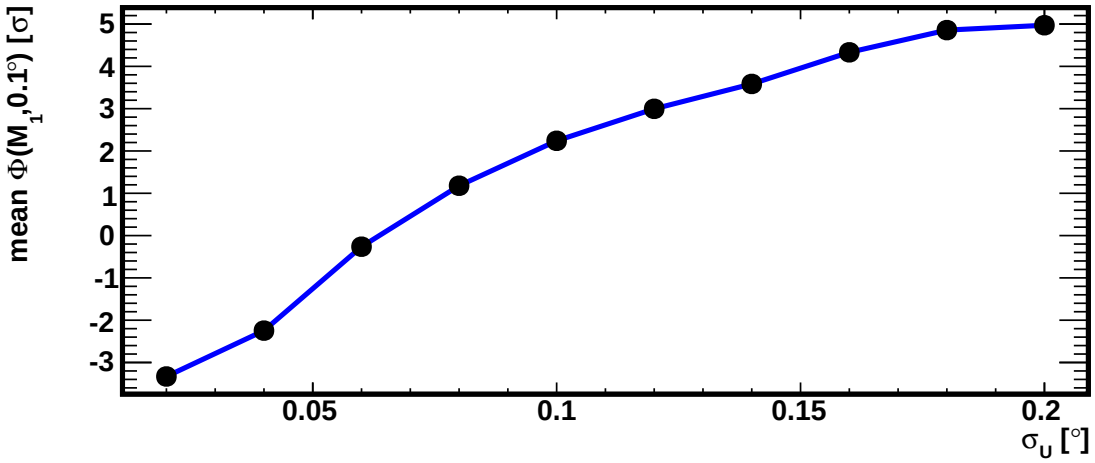

(c) sampled from smoothed map

Figure 3.14: maps without the two strong point sources (⇒ no exclusion regions)

3.2.5 Conclusion

There are two reasons why randomizing a map influences the correlation function:

1. events leave the exclusion regions
2. large-scale structures are destroyed

The radii for the exclusion regions will be $r_1 = r_2 = 0.3°$, because they contain most of the events of the two strong point sources, while not masking too many of the other events. The analysis indicates that for these radii the recommended range for randomization parameters is

- $\sigma_S < 0.12°$ for scattering in longitude and latitude,
- $\sigma_T < 0.12°$ for scattering in longitude only and
- $\sigma_U = [0.08°, 0.12°]$ for sampling from the smoothed map.

In the following, $\sigma_S = \sigma_T = \sigma_U = 0.1°$ will be used.

3.3 Analyzing artificial H_1 maps with weak source populations

First, an H_1 map is created, like before, by distributing events according to the exposure map and the density of the molecular cloud, plus two strong point sources added at the same location as in the data. Then, some weak sources are distributed on the map. Again, the number of events on this H_1 map is approximately the number of events in the data.

3.3.1 Source modeling

The sources are assumed to be point-like and their strengths and positions should be distributed like the already known sources.

The number of sources N with strength S follows a $log(N)$-$log(S)$ distribution

$$N(S) = S^{-\gamma}\,,$$

which will be used to sample source strengths from (see figure 3.15 (a)). As the generation of extremely strong sources, which are not in the data set anyway, has to be avoided, there will be a cutoff at a maximal source strength of $S_1 = 120$. With the median source strength $\overline{S}$ also given, the minimal source strength S_0 can be calculated to:

$$\begin{aligned} S_0 &= (2\overline{S}^{2-\gamma} - S_1^{2-\gamma})^{\frac{1}{2-\gamma}}\,, \text{ because} \\ \int_{S_0}^{\overline{S}} N(S)\,S\,\mathrm{d}S &= \frac{1}{2}\int_{S_0}^{S_1} N(S)\,S\,\mathrm{d}S\,. \end{aligned}$$

Figure 3.15 (a) shows the distribution the source strengths are sampled from for $\gamma = 3$ and $\overline{S} = 80$.
The latitude distribution of the Galactic VHE-γ-ray sources that have been found so far (see figure 3.15 (b)) will be used to sample the source positions in latitude; the longitudes positions are equally probable. There are no constraints on the distance between two sources, so it is possible that several sources overlap.

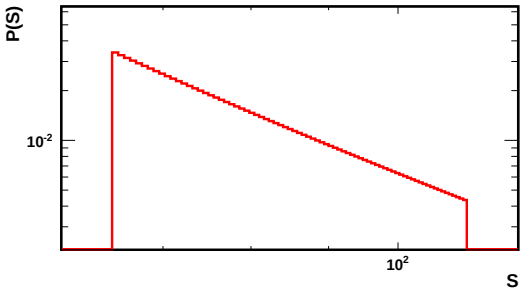

(a) Example distribution of source strengths for $\gamma = 3$, $\overline{S} = 80$ and $S_1 = 120$

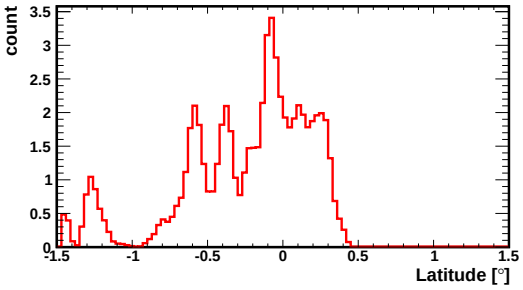

(b) Latitude distribution (smoothed) of known VHE-γ-ray sources on the Galactic Plane

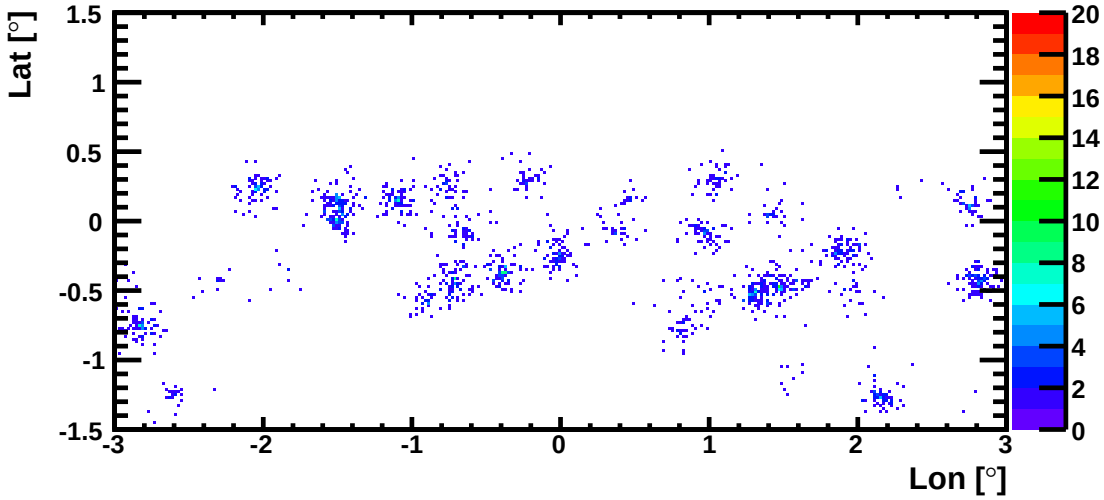

(c) Example map with sources generated according to (a) and (b)

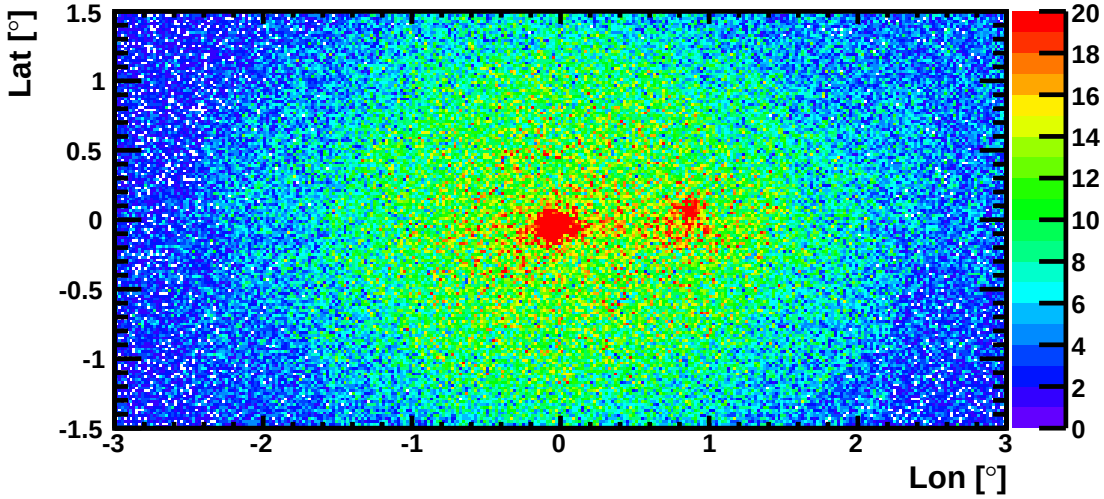

(d) Example of a final H_1 map containing background events due to exposure, events from diffuse emission, the two string point sources and several weak point sources

Figure 3.15: Sampling source positions and strengths

3.3.2 Results

Figure 3.16 (see detailed description there) shows the histogrammed values of the correlations functions at $r = 0.1^\circ$ for different numbers of sources and different randomization algorithms with randomization parameters $\sigma_S = \sigma_T = \sigma_U = 0.1^\circ$. The red histogram shows Φ for H_1 maps and the black histogram shows Φ for H_0 maps, which are obtained by applying the randomization operators S, T and U to the H_1 maps.

With the more complex and realistic background and source distributions models, the event correlation method is still sensitive to populations of weak sources and benefits from an increased number of sources, while the ring background method does not (see figure 3.17 for an exemplary comparison using randomization operator S (lon-lat-scattering) for the generation of H_0 maps).

The results presented in figure 3.18 indicate the properties of the source population (number of sources and mean source strength) required to affect the correlation function and the ring background method. If, for example, there are 50 sources in the data with a median source strength of 100 events, a $\sim 1.5\,\sigma$ detection is expected with the correlation method and $0\,\sigma$ with the ring background method.

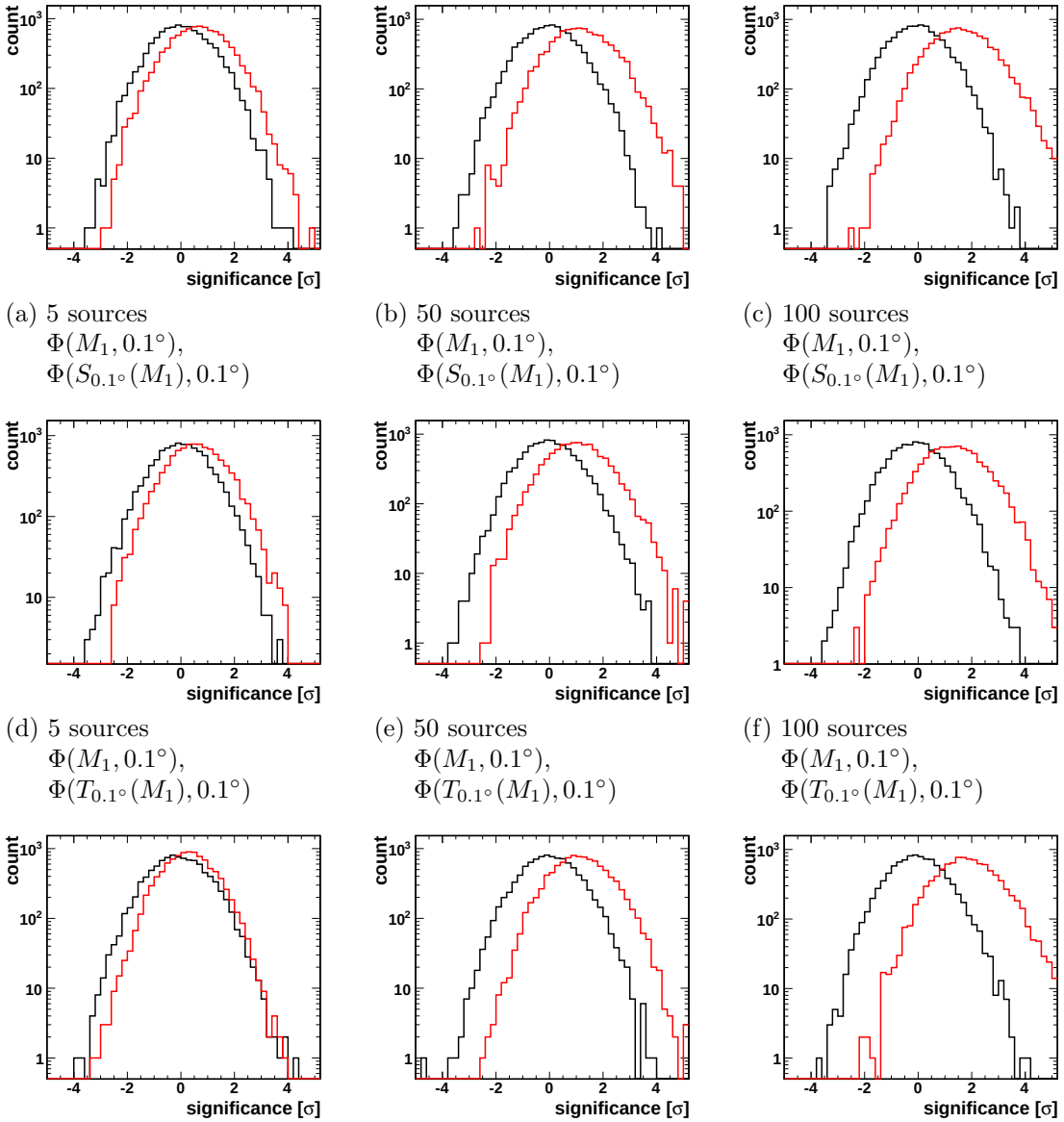

(a) 5 sources
$\Phi(M_1, 0.1°)$,
$\Phi(S_{0.1°}(M_1), 0.1°)$

(b) 50 sources
$\Phi(M_1, 0.1°)$,
$\Phi(S_{0.1°}(M_1), 0.1°)$

(c) 100 sources
$\Phi(M_1, 0.1°)$,
$\Phi(S_{0.1°}(M_1), 0.1°)$

(d) 5 sources
$\Phi(M_1, 0.1°)$,
$\Phi(T_{0.1°}(M_1), 0.1°)$

(e) 50 sources
$\Phi(M_1, 0.1°)$,
$\Phi(T_{0.1°}(M_1), 0.1°)$

(f) 100 sources
$\Phi(M_1, 0.1°)$,
$\Phi(T_{0.1°}(M_1), 0.1°)$

(g) 5 sources
$\Phi(M_1, 0.1°)$,
$\Phi(U_{0.1°}(M_1), 0.1°)$

(h) 50 sources
$\Phi(M_1, 0.1°)$,
$\Phi(U_{0.1°}(M_1), 0.1°)$

(i) 100 sources
$\Phi(M_1, 0.1°)$,
$\Phi(U_{0.1°}(M_1), 0.1°)$

Figure 3.16: Correlation functions at $r = 0.1°$ for H_1 maps with different numbers of sources (red) compared to the corresponding H_0 maps created from them (black) with $\sigma_S = \sigma_T = \sigma_U = 0.1°$. The values of the correlation functions are histogrammed after normalization to $\mu = 0$ and $\sigma = 1$ for H_0 maps, thus yielding significances.
The mean number of events per source is $\overline{S} = 80$ and the exclusion radii around the positions of Sagittarius A* and G 0.9+0.1 are $r_1 = r_2 = 0.3°$.

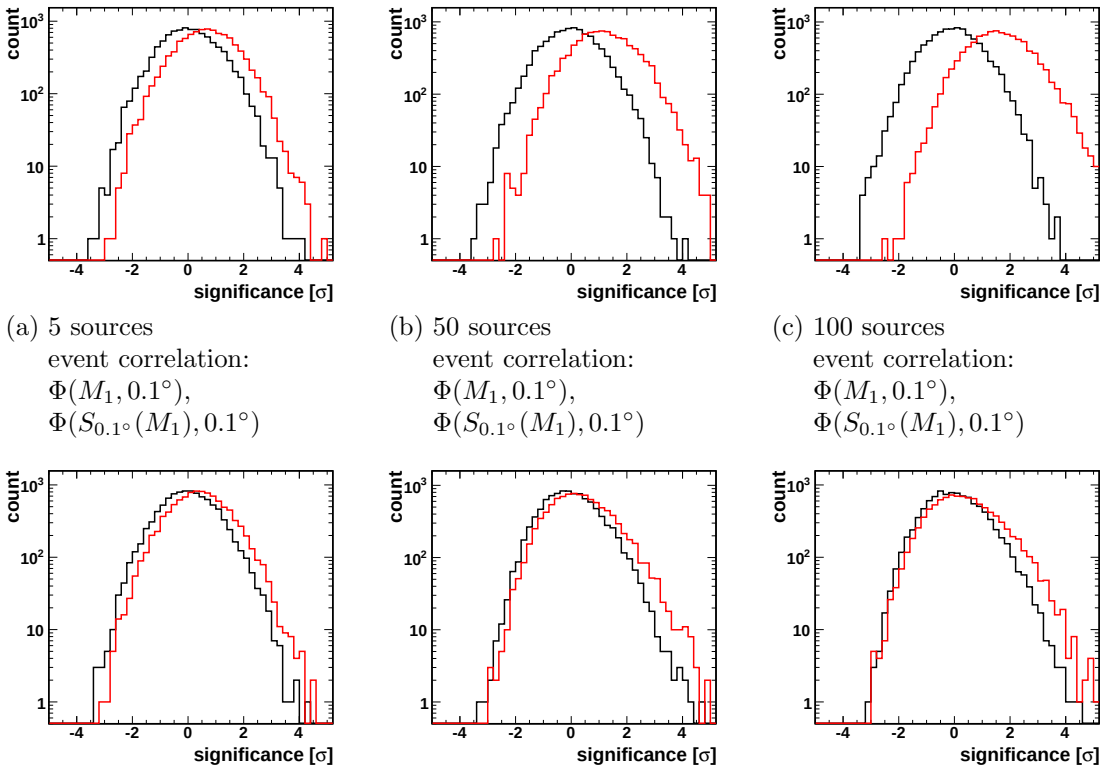

(a) 5 sources
event correlation:
$\Phi(M_1, 0.1^\circ)$,
$\Phi(S_{0.1^\circ}(M_1), 0.1^\circ)$

(b) 50 sources
event correlation:
$\Phi(M_1, 0.1^\circ)$,
$\Phi(S_{0.1^\circ}(M_1), 0.1^\circ)$

(c) 100 sources
event correlation:
$\Phi(M_1, 0.1^\circ)$,
$\Phi(S_{0.1^\circ}(M_1), 0.1^\circ)$

(d) 5 sources
ring background maximum significance M_1 and $S_{0.1^\circ}(M_1)$ (normalized)

(e) 50 sources
ring background maximum significance of M_1 and $S_{0.1^\circ}(M_1)$ (normalized)

(f) 100 sources
ring background maximum significance M_1 and $S_{0.1^\circ}(M_1)$ (normalized)

Figure 3.17: Comparison of event correlation to ring background for scattering in longitde and latitude with $\sigma_S = 0.1^\circ$. Top row: Correlation functions at $r = 0.1^\circ$ for H_1 maps with different numbers of sources (red) compared to the corresponding H_0 maps. The values of the correlation functions are histogrammed after normalization to $\mu = 0$ and $\sigma = 1$ for H_0 maps, thus yielding significances.
Bottom row: maximum significances obtained with the ring background method, normalized to $\mu = 0$ and $\sigma = 1$ for H_0 maps.
The mean number of events per source is $\overline{S} = 80$ and exclusion radii are $r_1 = r_2 = 0.3^\circ$.

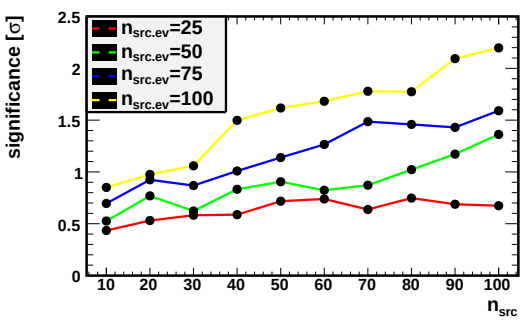

(a) lon-lat scattering with $\sigma_S = 0.1°$ event correlation

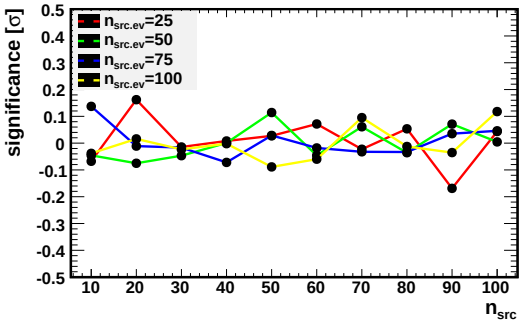

(b) lon-lat scattering with $\sigma_S = 0.1°$ ring background

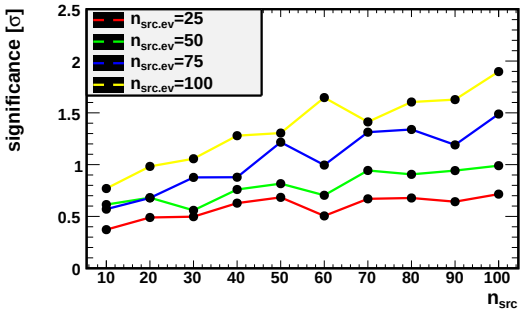

(c) lat scattering with $\sigma_T = 0.1°$ event correlation

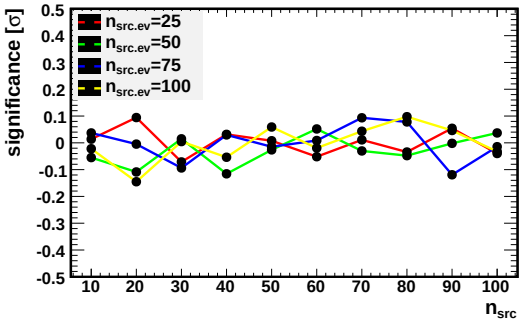

(d) lat scattering with $\sigma_T = 0.1°$ ring background

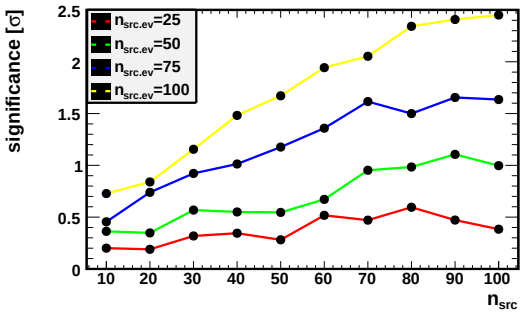

(e) sampled from map with $\sigma_U = 0.1°$ event correlation

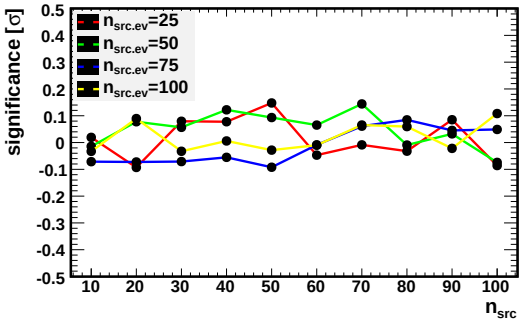

(f) sampled from map with $\sigma_U = 0.1°$ ring background

Figure 3.18: Mean significances obtained from the correlation function for different randomization methods, mean source strengths $n_{\mathrm{src.ev}}$ and number of sources n_{src}.

3.4 Analyzing the data

For the analysis of the data, regions with radii $r_1 = r_2 = 0.3°$ around Sagittarius A* and G 0.9+0.1 are excluded.
Figure 3.19 shows the result of the analysis for the three randomization methods with randomization parameters $\sigma_S = \sigma_T = \sigma_U = 0.1°$. The black histogram shows the value of the correlation function at $r = 0.1°$ for randomized maps, normalized to $\mu = 0$ and $\sigma = 1$ for the correlation functions of the randomized maps and the red bar shows the value of the correlation function at $r = 0.1°$ for the data, normalized in the same way. As the previous simulations have shown, small-scale anisotropies in the data would have caused the red bar being far more right. Instead, it lies near $0\,\sigma$, which means that randomizing the data has no effect on the correlation function, so there are probably no small-scale anisotropies in the data.

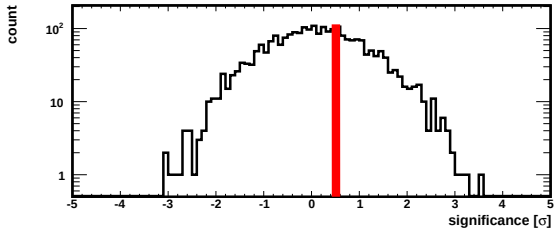

(a) $\Phi(\text{data}, 0.1°)$, $\Phi(S_{0.1°}(\text{data}), 0.1°)$

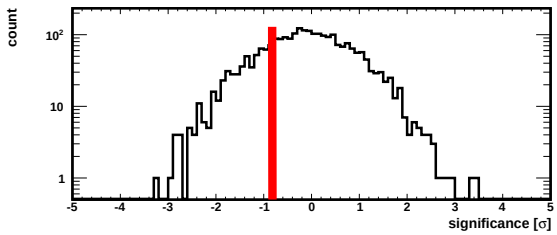

(b) $\Phi(\text{data}, 0.1°)$, $\Phi(T_{0.1°}(\text{data}), 0.1°)$

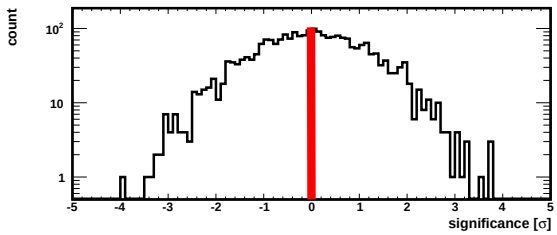

(c) $\Phi(\text{data}, 0.1°)$, $\Phi(U_{0.1°}(\text{data}), 0.1°)$

Figure 3.19: Value of the correlation function at $r = 0.1°$ for the data (red) normalized with regard to maps randomized by different methods (black). From top to bottom: scattering in longitude and latitude, scattering in latitude only, sampling from smoothed map.

4 Conclusion

4.1 Summary

An event correlation method has been introduced and applied to the analysis of γ-ray maps of the Galactic Centre. In order to obtain the necessary H_0 maps, different methods for the destruction of small-scale structures have been analyzed and then used on the data. Monte Carlo simulations have been conducted to verify that the exclusion regions and randomization strengths used in the analysis do not change the large-scale distribution of the event map. To the event correlation method, the data appears to be as random as the randomized data, so there are no small-scale anisotropies, which means that there is no indication for populations of weak point sources and thus, the observed γ-rays arriving from the Galactic Centre region are consistent with diffuse emission.

4.2 Outlook

Improved scattering

To allow stronger randomization, events could be scattered along the lines and areas of equal density. Those lines are all positions where the $\Delta(M) = 0$.

Weighted correlation function

A different correlation function, which is especially sensitive on point sources with $\sigma_{\mathrm{pdf}} = 0.1^\circ$ could improve the analysis. Tests on artificial maps have shown that it is more sensitive than the normal event correlation method.

Local anisotropy

Since H_0 maps have an isotropic event distribution in a small circle ($r \leq 0.1^\circ$) around every position on the map, another way to distinguish H_1 maps from H_0 maps is to measure how much these local event distributions of the H_1 map differ from an isotropic distribution that has the same number of events:

$$s = \sum_{i=1}^{n} \left| f(M_1^i), f(E(M_1^i)) \right| ,$$

where f is a function that measures the anisotropy in a small circle around event i and E is an operator that equally distributes the same number of events in a circle of the same size.

Other

The same analysis can soon be done with data from H.E.S.S. 2. Also, the analysis could be done depending on energy ranges.

4.3 Acknowledgements

I thank

- Prof. Bloch and Prof. Dubuisson for allowing me to write this thesis and always helping me with all the administrative and technical questions at once, even if the questions weren't part of the thesis.
- Prof. Hofmann for accepting me as his student, for giving me such an interesting topic, excellent work environment, good advices and ideas and for never having no time for me, although he never has time
- Henning for the many hours of thorough explanations, for helping me nearly every day, for providing me with papers and data and for giving me the answers to my questions so quickly. I am glad he was my supervisor and it is a pity that he leaves the group.
- Willi for the interesting explanations on astrophysics and the respectable supervision during the conferences

I assure that I wrote all the code and this text on my own.

Bibliography

[1] F. Aharonian et al. Very high energy gamma rays from the direction of Sagittarius A*. *A&A*, 425:L13–L17, October 2004. doi: 10.1051/0004-6361:200400055.

[2] F. Aharonian et al. Very high energy gamma rays from the composite SNR G 0.9+0.1. *A&A*, 432:L25–L29, March 2005. doi: 10.1051/0004-6361:200500022.

[3] F. Aharonian et al. Discovery of very-high-energy γ-rays from the Galactic Centre ridge. *Nature*, 439:695–698, February 2006. doi: 10.1038/nature04467.

[4] F. Aharonian et al. The H.E.S.S. Survey of the Inner Galaxy in Very High Energy Gamma Rays. *ApJ*, 636:777–797, January 2006. doi: 10.1086/498013.

[5] D. Berge, S. Funk, and J. Hinton. Background modelling in very-high-energy γ-ray astronomy. *A&A*, 466:1219–1229, May 2007. doi: 10.1051/0004-6361:20066674.

[6] H. Gast et al. Exploring the Galaxy at TeV energies: Latest results from the H.E.S.S. Galactic Plane Survey. In *32nd International Cosmic Ray Conference, Beijing 2011*, 2011.

[7] Andrea Goldwurm. An overview of the high-energy emission from the Galactic Center. In D. Q. Wang M. Morris and F. Yuan, editors, *Invited paper at the Galactic Center Workshop 2009, Shanghai, to appear in T̈he Galactic Center: A Window on the Nuclear Environment of Disk Galaxies¨*, 2010.

[8] T.-P. Li and Y.-Q. Ma. Analysis methods for results in gamma-ray astronomy. *ApJ*, 272:317–324, September 1983. doi: 10.1086/161295.

[9] Yolanda Sestayo de la Cerra. Search for high energy neutrinos from our Galaxy with IceCube. In *Ph.D. thesis, Universität Heidelberg*, pages 1–119, 2010.

[10] M. Tsuboi, T. Handa, and N. Ukita. Dense Molecular Clouds in the Galactic Center Region. I. Observations and Data. *ApJS*, 120:1–39, January 1999. doi: 10.1086/313165.